Original Article

Identification key genes, key miRNAs and key transcription factors of lung adenocarcinoma

Jinghang Li, Zhi Li, Sheng Zhao, Yuanyuan Song, Linjie Si, Xiaowei Wang

Department of Cardiovascular Surgery, The First Affiliated Hospital of Nanjing Medical University, Nanjing 210029, China

Contributions: (I) Conception and design: X Wang; (II) Administrative support: S Zhao; (III) Provision of study materials or patients: J Li; (IV) Collection and assembly of data: J Li; (V) Data analysis and interpretation: J Li; (VI) Manuscript writing: All authors; (VII) Final approval of manuscript: All authors.

Correspondence to: Xiaowei Wang, MD, PhD. Department of Cardiovascular Surgery, The First Affiliated Hospital of Nanjing Medical University, The Guangzhou Road Number 300, Nanjing 210029, China. Email: wangxiaowein1@163.com.

Background: Lung adenocarcinoma (LUAD) is one of the most common cancers worldwide. The etiology and pathophysiology of LUAD remain unclear. The aim of the present study was to identify the key genes, miRNAs and transcription factors (TFs) associated with the pathogenesis and prognosis of LUAD.

Methods: Three gene expression profiles (GSE43458, GSE32863, GSE74706) of LUAD were obtained from the Gene Expression Omnibus (GEO) database. Differentially expressed genes (DEGs) were identified by GEO2R.The Gene Ontology (GO) terms, pathways, and protein-protein interactions (PPIs) of these DEGs were analyzed. Bases on DEGs, the miRNAs and TFs were predicted. Furthermore, TF-gene-miRNA co-expression network was constructed to identify key genes, miRNAs and TFs by bioinformatic methods. The expressions and prognostic values of key genes, miRNAs and TFs were carried out through The Cancer Genome Atlas (TCGA) database and Kaplan Meier-plotter (KM) online dataset.

Results: A total of 337 overlapped DEGs (75 upregulated and 262 downregulated) of LUAD were identified from the three GSE datasets. Moreover, 851 miRNAs and 29 TFs were identified to be associated with these DEGs. In total, 10 hub genes, 10 key miRNAs and 10 key TFs were located in the central hub of the TF-gene-miRNA co-expression network, and validated using The Cancer Genome Atlas (TCGA) database. Specifically, seven genes (*PHACTR2*, *MSRB3*, *GHR*, *PLSCR4*, *EPB41L2*, *NPNT*, *FBXO32*), two miRNAs (hsa-let-7e-5p, hsa-miR-17-5p) and four TFs (STAT6, E2F1, ETS1, JUN) were identified to be associated with prognosis of LUAD, which have significantly different expressions between LUAD and normal lung tissue. Additionally, the miRNA/gene co-expression analysis also revealed that hsa-miR-17-5p and PLSCR4 have a significant negative co-expression relationship (r=–0.33, P=1.67e-14) in LUAD.

Conclusions: Our study constructed a regulatory network of TF-gene-miRNA in LUAD, which may provide new insights about the interaction between genes, miRNAs and TFs in the pathogenesis of LUAD, and identify potential biomarkers or therapeutic targets for LUAD.

Keywords: Lung adenocarcinoma (LUAD); TF-gene-miRNA co-expression network; bioinformatical analysis; Kaplan-Meier analysis

Submitted Dec 27, 2019. Accepted for publication Mar 27, 2020.
doi: 10.21037/jtd-19-4168
View this article at: http://dx.doi.org/10.21037/jtd-19-4168

Introduction

Lung cancer is one of the most common cancers and the leading causes of cancer-related death worldwide (1). Lung adenocarcinoma (LUAD) is a major histological type of lung cancer. Despite recent advances in technology of molecular diagnosis and therapy, the prognosis of LUAD is still not optimistic, and the risk of metastasis and recurrence is still high (2). Therefore, it is necessary to search novel

© Journal of Thoracic Disease. All rights reserved.

biomarkers and therapy targets for LUAD diagnosis and prognosis.

Transcription factors (TFs), regulate gene expression by binding to specific DNA sequences at the transcriptional level, have an important role in the pathogenesis and development of cancer. The recent study showed that four TFs (ASCL1, NeuroD1, YAP1 and POU2F3) play critical roles in small cell lung cancer (3). The TF family p53/p63/p73 plays a critical role in Squamous Cancer Pathogenesis by regulating homeostasis of squamous epithelium (4).

MicroRNAs (miRNAs) are endogenous small non-coding RNAs (18–22 nucleotide-long) that mainly inhibit gene expression at the post-transcriptional level by directly binding to the 3'UTR of the target mRNAs. MiRNAs play an important role in regulating a range of biological functions, including proliferation, apoptosis, cell survival, tumor growth and metastasis. Several miRNAs have been identified as novel biomarkers and therapy targets of cancer in recent years (5-7). For example, microRNA-193b, act as a tumor suppressor, have antileukemic efficacy and can improve prognostic of acute myeloid leukemia (8).

Both TFs and miRNAs play critical roles in the regulation of mRNAs and participate in the pathogenesis of cancer. It is important to unravel the interaction of TFs, miRNAs, and gene within TF-gene-miRNA regulatory network, which would helpful to discover novel biomarkers and therapy targets of cancer (9,10).

In this study, three gene expression profiles [GSE43458 (11), GSE74706 (12), GSE32863 (13)] of LUAD were analyzed to obtain DEGs between LUAD tissues and normal tissues by GEOR2.The functions, pathways and PPI network analysis of DEGs were performed. Then, the target miRNAs and TFs of DEGs were predicted by bioinformatic methods. Finally, the TF-gene -miRNA co-expression network was established to investigate the interaction between genes, miRNAs and TFs in the pathogenesis of LUAD, and identify key genes, miRNAs and TFs in LUAD.

Methods

Microarray data collection and screen of DEGs

Three gene expression profiles of LUAD (GSE43458, GSE32863, GSE74706) were obtained from Gene Expression Omnibus (https://www.ncbi.nlm.nih.gov/geo/). The GSE43458 [(HuGene-1_0-st) Affymetrix Human Gene 1.0 ST Array (transcript (gene) version)] dataset included 30 normal lung tissues and 80 LUAD tissues. The GSE32863 (Illumina HumanWG-6 v3.0 expression bead chip) dataset included 58 LUAD tissues and 58 adjacent non-tumor lung tissues. The GSE74706 (Agilent-026652 Whole Human Genome Microarray 4x44K v2) dataset contain 18 normal lung tissues and 18 LUAD tissues. GEOR2 (https://www.ncbi.nlm.nih.gov/geo/geo2r/), an online tool of Gene Expression Omnibus, was used to screen DEGs from the gene expression data. DEGs were screened with the criteria of adjust P value <0.05 and |logFC| >1, and overlapped upregulated and downregulated DEGs were obtained respectively.

Functional annotation and pathway enrichment analysis

To explore the function of a large scale of genes, the Gene Ontology (GO) term enrichment analysis and Reactome pathway analysis of upregulated and downregulated DEGs were respectively conducted by using CluoGO APP of Cytoscape software platform (14). P<0.05 as the cut-off criterion of both GO and pathway analysis.

Construct PPI network of the DEGs

The PPI network, which can visualize the interaction and reveal the relationship between each proteins, was constructed by The Search Tool for the Retrieval of Interacting Genes/Proteins (STRING) (http://string-db.org) (15) with the threshold of minimum required interaction score >0.7. The PPI network was visualized and further analyzed using Cytoscape software platform (14). Two kinds of analysis methods were induced to investigate key nodes of the PPI network. One method was to identify hub modules of the network by using a plug-in of Cytoscape software platform, which called MCODE with criteria of maximum depth from Seed =100, k-core =2, node score Cutoff =0.2 and degree >5. Another method was using cytoHubba, which could rank the nodes according to the properties of nodes, and top 20 nodes were selected.

TF-gene-miRNA co-expression network construction

Target miRNAs of DEGs were predicted by an online tool called miRWalk (http://zmf.umm.uni-heidelberg.de/apps/zmf/mirwalk/) (16) in two miRNA databases (TargetScan and miRDB) with the cutoff value binding score >0.95, the miRNAs identified in both two databases were considered as target miRNAs. The target TFs of DEGs were predicted

© Journal of Thoracic Disease. All rights reserved.

by TRRUST (https://www.grnpedia.org/trrust/) (17), which is a database of human TF networks, with the criteria of P value <0.05. Then a TF-gene-miRNA co-expression network was constructed, visualized and further analyzed using Cytoscape. In order to explore the hub nodes in TF-gene-miRNA co-expression network, a plug-in of Cytoscape called cytoHubba was used, which can rank the nodes according to the properties of nodes. It provides 11 kinds topological analysis methods including MCC, DMNC, MNC, Degree, EPC and so on. The Degree topological analysis method was used because the degree of a node is directly related to its genetic importance; in other words, a node with a high degree tends to be a key node. According to the nodes' degree value, top 10 genes, 10 miRNAs and 10 TFs was selected as hub nodes for further investigation.

Validations and Kaplan-Meier survival analysis of the hub nodes

We verified the differential expressions of these hub genes and TFs using GEPIA (http://gepia.cancer-pku.cn/index.html) (18), which is an interactive web that includes 9,736 tumors and 8,587 normal samples from TCGA and the GTEx projects. The criteria of DEGs was adjust P value <0.001 and |logFC| >1. We also verified the differential expressions of these miRNAs using starBase (http://starbase.sysu.edu.cn/index.php), which accompany with 10,546 miRNA-seq data of 32 types cancers. The cutoff criteria was adjust P value <0.05 and |logFC| >1. The relationship between the genes, miRNAs and TFs and the prognosis of LUAD was analyzed by Kaplan-Meier Plotter (http://kmplot.com/analysis/) (19), which contain 720 LUAD patients with detailed survival data. The threshold of significant association was log-rank P value <0.05. Furthermore, Human Protein Atlas (http://www.proteinatlas.org) was used to validate the protein level of hub genes and TFs in LUAD tissues and normal tissues.

Immunohistochemistry

In addition, we used paraffin samples from LUAD patients to verified the protein level of hub gene (FBXO32) by IHC (immunohistochemistry). The resected LUAD tissues were fixed with 10% neutral buffered formalin. The histological evaluation was performed on hematoxylin and eosin stained sections. The LUAD tissue sections were immunostained with primary antibodies against FBXO32 (Proteintech, China). After incubation with primary antibody, the detection of antibodies was accomplished using the streptavidin peroxidase method. Immunohistochemical scoring was based on the staining intensity and the percentage of positively stained cells. The staining intensity was scored as follows: 0, no staining; 1, weakly stained; 2, moderately stained; and 3, strongly stained. The data are presented as the mean ± standard deviation, and P<0.05 was considered significant.

The miRNA-gene co-expression in LUAD patients

The Pan-Cancer Analysis Platform of starBase (http://starbase.sysu.edu.cn/index.php) (20) is designed for decoding networks of noncoding RNAs, RNA-binding proteins and all protein-coding genes by analyzing the expression profiles across 32 cancer types from TCGA project, which provide exploration of co-expression networks of 2 candidate genes, including miRNA-RNA and RNA-RNA in 32 types of cancers. The co-expression between key miRNAs and genes was predicted by starBase.

Results

Identification of DEGs in LUAD

We identified 251, 493, 1,652 upregulated DEGs, and 646, 747, 2,439 downregulated DEGs in the GSE43458, GSE32863 and GSE74706 datasets respectively. A total of 75 upregulated DEGs (*Figure 1A*) and 262 downregulated DEGs (*Figure 1B*) overlapped across the three datasets (*Tables S1,S2*).

Functional annotation of overlapped DEGs

To further investigate the function of overlapped DEGs, the GO term and Reactome pathways enrichment analysis were performed. The most significantly enriched Reactome pathway of downregulated DEGs were extracellular matrix organization, semaphoring interactions, surfactant metabolism, complement cascade, regulation of complement cascade and biological oxidations (*Figure 2A*). The biological process of downregulated DEGs were significantly enriched in blood vessel development, angiogenesis and response to organic substance (*Figure 2B*). The most significantly enriched Reactome pathway of upregulated DEGs were cell cycle mitotic, collagen degradation and metabolism of amino acids and derivatives (*Figure 2C*); the biological

© Journal of Thoracic Disease. All rights reserved.

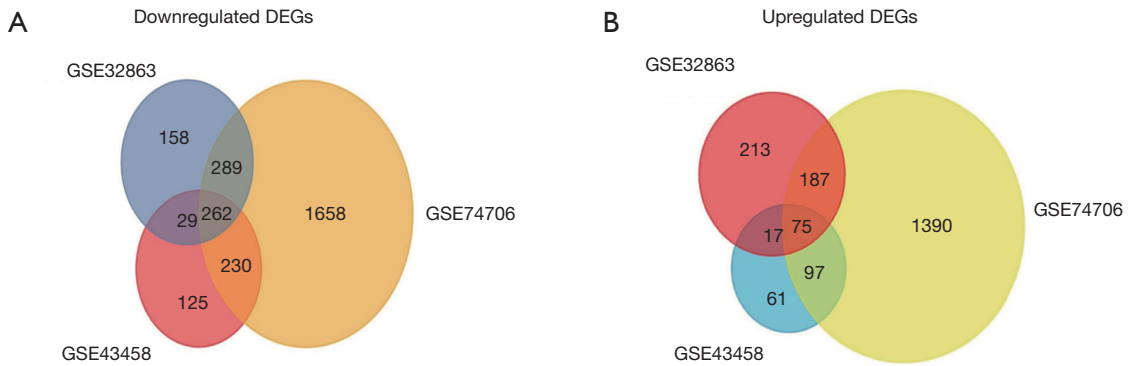

Figure 1 The overlapped DEGs of GSE43458, GSE32863 and GSE74706. The Venn diagram of overlapped downregulated DEGs of GSE43458, GSE32863 and GSE74706 (A). The Venn diagram of overlapped upregulated DEGs of GSE43458, GSE32863 and GSE74706 (B). DEGs, differentially expressed genes.

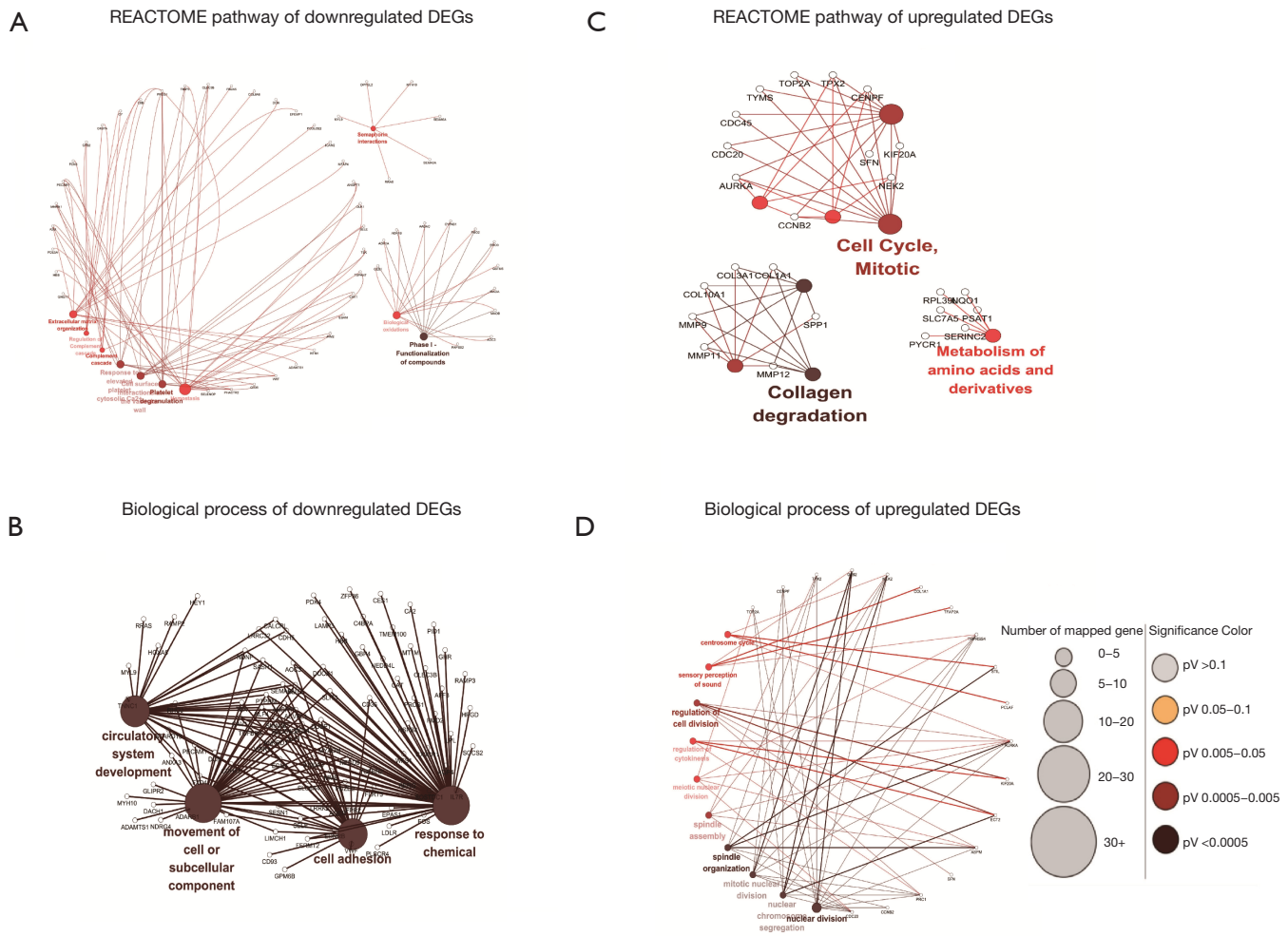

Figure 2 The functional annotation of overlapped DEGs. The most significantly enriched Reactome pathway of downregulated DEGs (A). The biological process (BP) of downregulated DEGs (B). The most significantly enriched Reactome pathway of upregulated DEGs (C). The BP of upregulated DEGs (D). DEGs, differentially expressed genes.

© Journal of Thoracic Disease. All rights reserved.

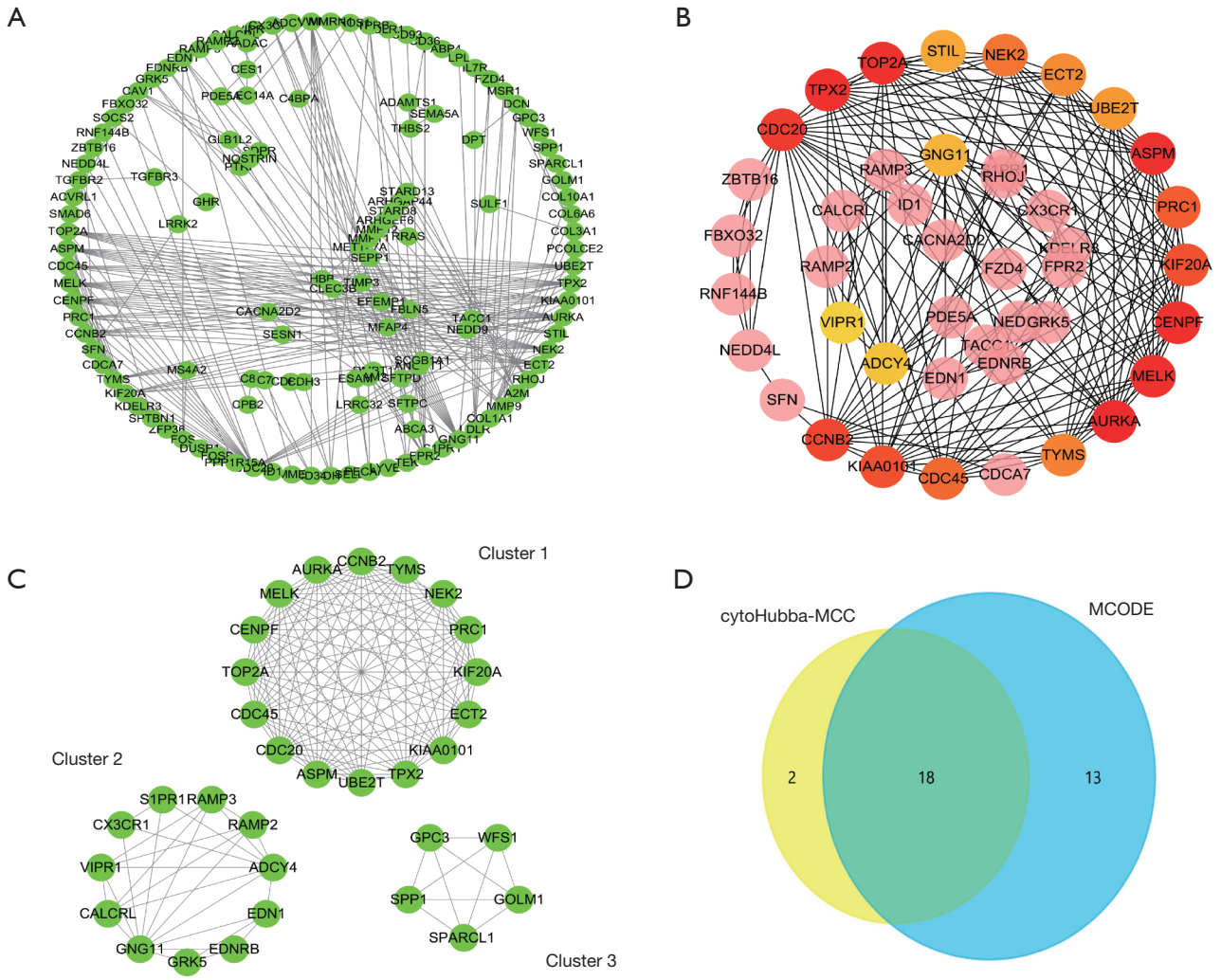

Figure 3 The PPI network of total DEGs with the threshold of minimum required interaction score >0.7 (A). The top 20 nodes of PPI network evaluated in cytoHubba MCC arithmetic (B). The top modules of PPI network evaluated in MOCDE with criteria of maximum depth from Seed =100, k-core =2, node score Cutoff =0.2 and degree >5 (C). The Venn diagram of common genes of two arithmetic (D). DEGs, differentially expressed genes.

process of upregulated DEGs were significantly enriched in movement of cell or subcellular component, response to chemical, circulator system development, cell adhesion (*Figure 2D*).

The PPI network and hub genes

262 downregulated overlapped DEGs and 75 upregulated overlapped DEGs were all filtered into the PPI network by using the STRING. A total of 337 nodes and 164 edges were obtained from the PPI network program. The average node degree was 2.14 and PPI enrichment P value was <1.0e-16, with the threshold of minimum required interaction score >0.7 (*Figure 3A* and *Table S3*). The PPI network was visualized and further analyzed using Cytoscape software platform. Two kinds of analysis methods were induced to investigate key nodes of the PPI network. The cytoHubba method identified top 20 nodes (*Figure 3B* and *Table S4*). The MCODE method identified 3 clusters of genes (*Figure 3C* and *Figure S1*). The 18 overlapped genes of these two methods were considered as hub nodes of the PPI network (*Figure 3D*).

© Journal of Thoracic Disease. All rights reserved.

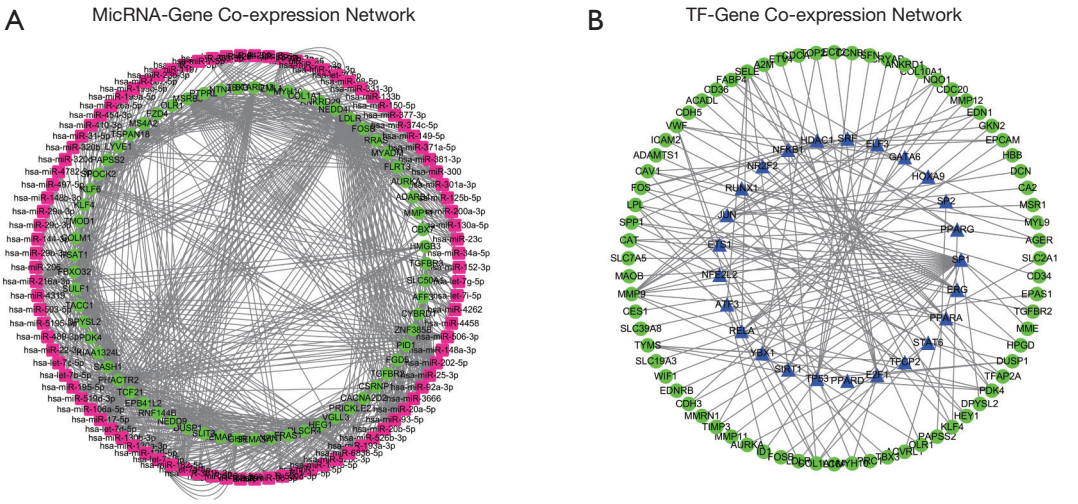

Figure 4 The miRNA-gene co-expression network. The purple squares represent microRNAs and the green circles represent genes (A). The TF-gene co-expression network. The blue triangles represent TFs and the green circles represent genes (B). TFs, transcription factors.

TF-gene-miRNA co-expression network construction

In two miRNA databases(TargetScan and miRDB), 851 overlapped target miRNAs of all 337 DEGs were obtained with the cutoff value Binding Score >0.95 (*Table S5*), and gene-miRNA co-expression network was constructed (*Figure 4A*). 29 TFs of all DEGs were obtained in TRRUST with the criteria of P value <0.05 (*Table S6*), and TF-gene co-expression network was constructed (*Figure 4B*). The TF-gene-miRNA co-expression network was constructed and the properties of each node in this co-expression network were calculated by cytoHubba (*Figure 5* and *Table S7*). According to the nodes' degree value, top 10 key genes (NEDD4L, LDLR, PHACTR2, MSRB3, GHR, PLSCR4, TSPAN18, EPB41L2, NPNT, FBXO32), 10 key miRNAs (hsa-miR-6838-5p, hsa-let-7e-5p, hsa-miR-17-5p, hsa-miR-216a-3p, hsa-miR-25-3p, hsa-let-7d-5p, hsa-miR-93-5p, hsa-miR-92b-3p, hsa-miR-92a-3p, hsa-miR-106a-5p) and 10 key TFs (SP1, ERG, PPARA, STAT6, E2F1, TP53, SIRT1, RELA, ETS1, JUN) was selected as hub nodes for further investigation.

Validations and Kaplan-Meier survival analysis of these hub nodes

We verified the differential expressions of these hub genes and TFs in 483 LUAD patients and paired 374 normal individuals with the GEPIA datasets. A total of eight genes (*LDLR*, *PHACTR2*, *MSRB3*, *GHR*, *PLSCR4*, *TSPAN18*, *EPB41L2* and *NPNT*) have significant lower expressions in LUAD patients, and FBXO32 had a significant higher expression in LUAD patients (*Figure 6*). In the Kaplan-Meier Plotter analysis, seven genes [*PHACTR2* (P=4.7e-10), *MSRB3* (P=6.2e-10), *GHR* (P=0.0018), *PLSCR4* (P=8.4e-10), *EPB41L2* (P=1.2e-5), *FBXO32* (P=0.037) and *NPNT* (P=4.2e-7)] were identified association with poor prognosis of LUAD (*Figure 7*). Additionally, four TFs (ERG, STAT6, ETS1 and JUN) have significant lower expressions in LUAD patients, and E2F1 has a significant higher expression in LUAD patients (*Figure 8*). In the Kaplan-Meier Plotter analysis, four TFs [STAT6 (P=7.7e-9), ETS1 (P=2e-13), JUN (P=0.0026) and E2F1 (P=5e-9)] show significant association with prognosis of LUAD (*Figure 9*).

Next, we used starBase database to validate the differential expressions of key miRNAs in 521 LUAD patients and 20 paired normal individuals. Two miRNAs [hsa-let-7e-5p (P=4.2e-5) and hsa-let-7d-5p (P=0.00077)] have significant lower expressions in LUAD patients, and four miRNAs [hsa-miR-17-5p (P=2.4e-19), hsa-let-25-3p (P=0.047), hsa-miR-93-5p (P=2e-11) and hsa-miR-106a-5p (P=1.7e-18)] have significant higher expressions (*Figure 10*). In the Kaplan-Meier Plotter analysis, two miRNAs [hsa-let-7e (P=0.011) and hsa-let-17 (P=0.035)] show significant association with poor prognosis of LUAD (*Figure 11*).

To further demonstrate that the hub genes and key TFs were related to LUAD, we used The Human Protein Atlas database(www.proteinatlas.org) to verify the protein expression of key genes and key TFs. Compared to normal

© Journal of Thoracic Disease. All rights reserved.

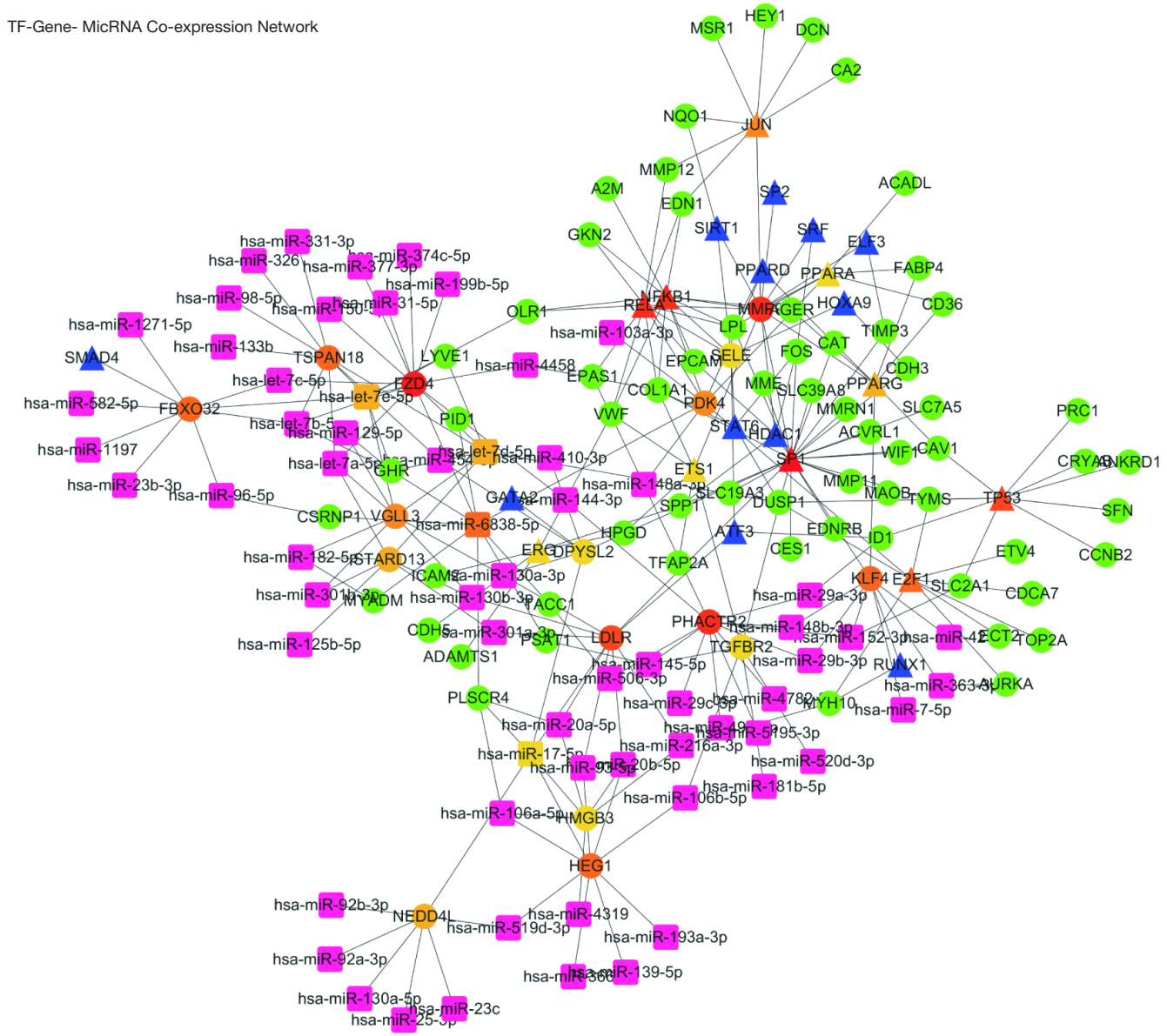

Figure 5 The TF-gene- miRNA co-expression network and hub nodes of this network. The purple squares represent microRNAs, the green circles represent genes and the blue triangles represent TFs. The degree value of each node in this co-expression network were calculated by cytoHubba, the color of the nodes from red to yellow means the degree value of the node from large to small.

lung tissues, the protein expressions of 6 hub genes (*PHACTR2*, *MSRB3*, *GHR*, *PLSCR4*, *EPB41L2*, *NPNT*) and 3 key TFs (STAT6, ETS1 and JUN) in LUAD tissues were significantly lower, and the protein expression of the key TF (E2F1) in LUAD tissues were significantly higher (*Figures S2,S3*). Immunohistochemistry staining obtained from The Human Protein Atlas database contain 6 key genes and 4 TFs, while the hub gene (*FBXO32*) was not included in the website. Therefore, we verified the protein expression level of FBXO32 in LUAD tissues by IHC. The result showed that FBXO32 protein expression level was significantly increased in LUAD tissues compared to that in normal lung tissues (*Figure S4*). These results showed that the protein levels of these key genes and TFs were

© Journal of Thoracic Disease. All rights reserved.

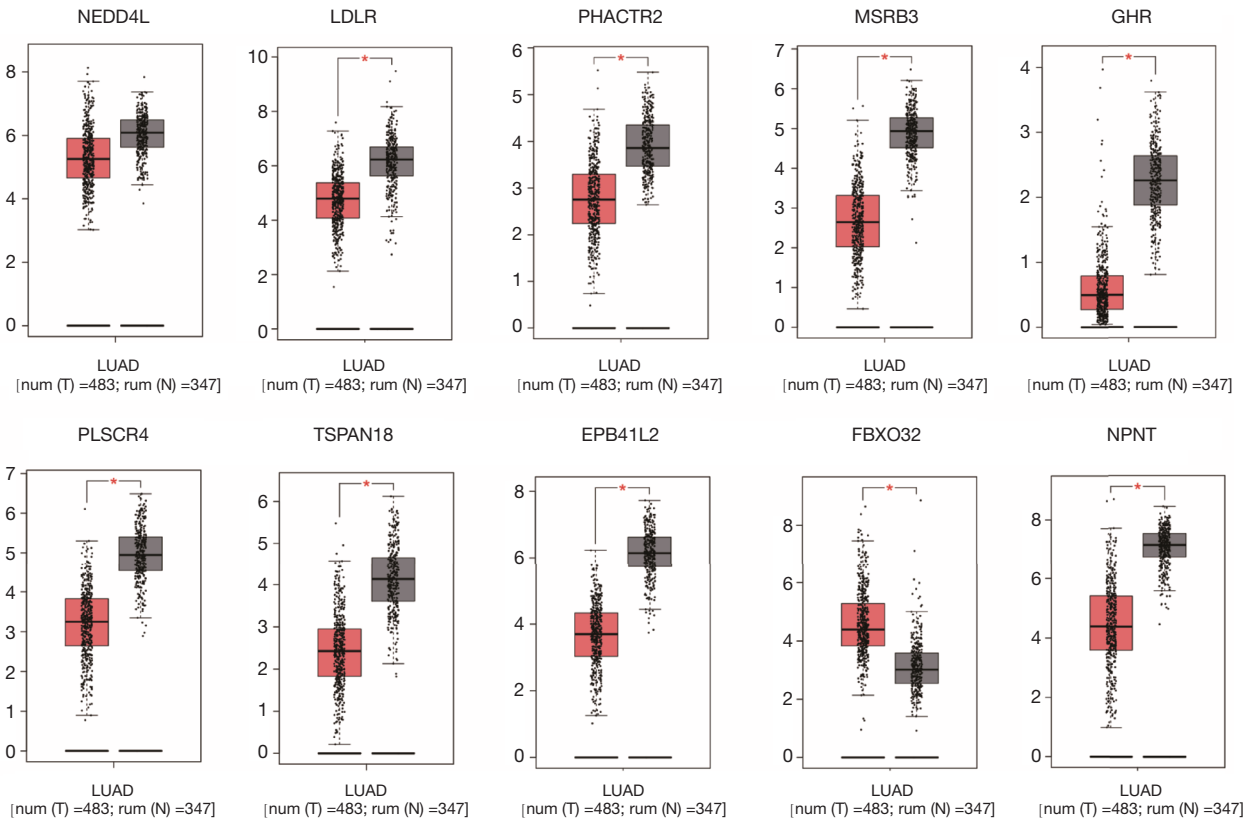

Figure 6 The expression of top 10 hub genes in GEPIA datasets. The red bars represent tumor samples, the gray bars represent normal samples and the red asterisk means a significant differential expression.

consistent with mRNA levels.

The miRNA-gene co-expression in LUAD patients

The co-expression between key miRNAs and genes in LUAD was predicted by starBase. The results shown that hsa-miR-17-5p and PLSCR4 have a significant negative co-expression (r=–0.33, P=1.67e-14) (*Figure 12*). Moreover, hsa-miR-17-5p have a binding site with PLSCR4 predicted by starBase (*Figure S5*).

Discussion

LUAD is the major histological type of lung cancers. Although great improvement has been achieved in the treatments of LUAD, the prognosis of LUAD is still not optimistic. The progress of genomic medicine has improved the treatment outcomes and life quality of LUAD patients compared to traditional chemotherapy (21). In recent years, due to the advances in the knowledge of pathways and related genetic mutations, several drugs targeting the major pathways have been identified (22,23). The common pathways are NTRK/ROS1, EGFR, RAS-MAPK and PI3K/AKT/mTOR pathways (24,25). Many drugs targeting the genetic mutations of these pathways have been developed and shown great therapeutic values, such as EGFR inhibitors gefitinib and erlotinib, NTRK/ROS1 inhibitors entrectinib (25,26). Some of these drugs have become first line treatment and replaced chemotherapy (22). Despite the tremendous progress have made in the treatment of LUAD with target drugs, drug resistance remains a prominent and inevitable problem. Therefore, it is necessary to research novel therapy targets of LUAD. Gene chip and bioinformatic technology facilitates the exploration of new therapeutic targets in many diseases.

In present study, three gene express profile datasets of LUAD were obtained from GEO database, including 106 normal lung tissues and 156 LUADs tissues. A total of 75 upregulated overlapped DEGs and 262 downregulated overlapped DEGs were identified. We then performed

© Journal of Thoracic Disease. All rights reserved.

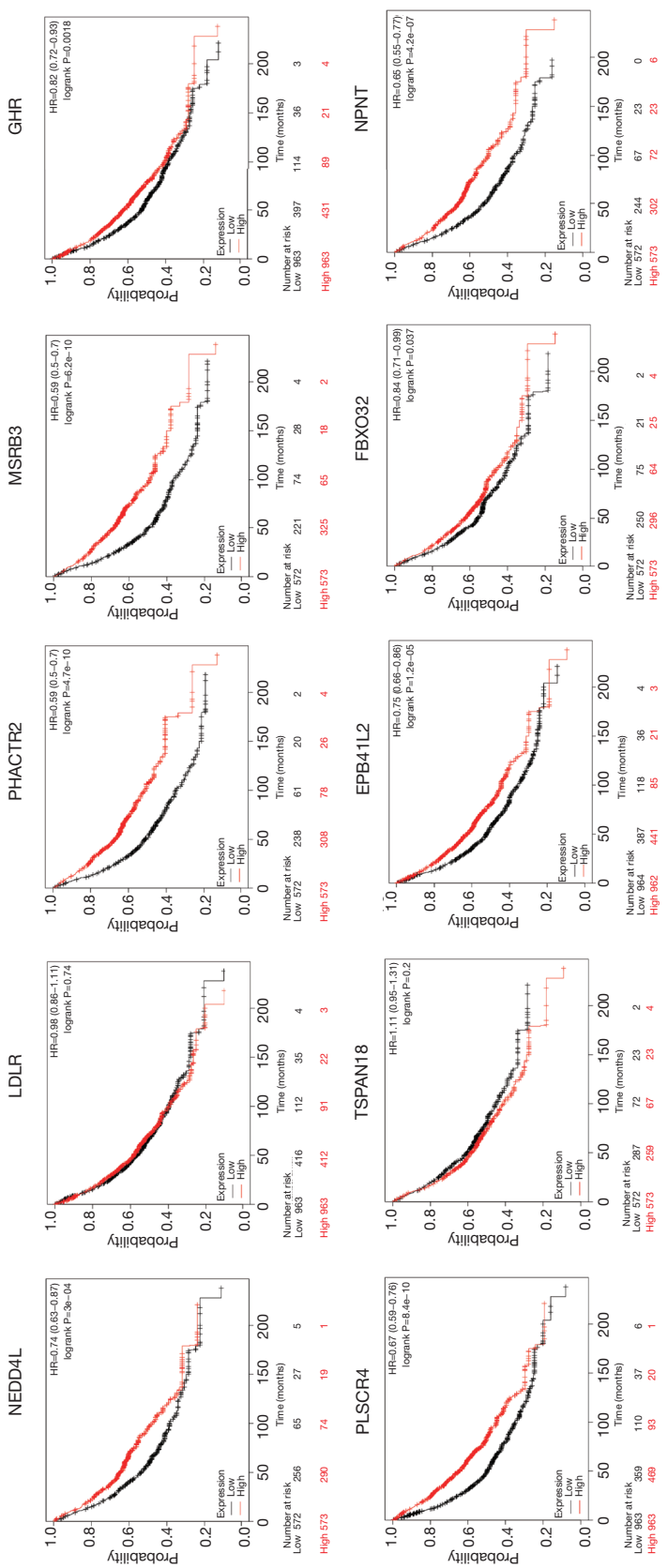

Figure 7 The prognosis value of 10 hub genes in the Kaplan-Meier Plotter analysis. The red lines represent high expression samples, the black lines represent low expression samples.

© Journal of Thoracic Disease. All rights reserved.

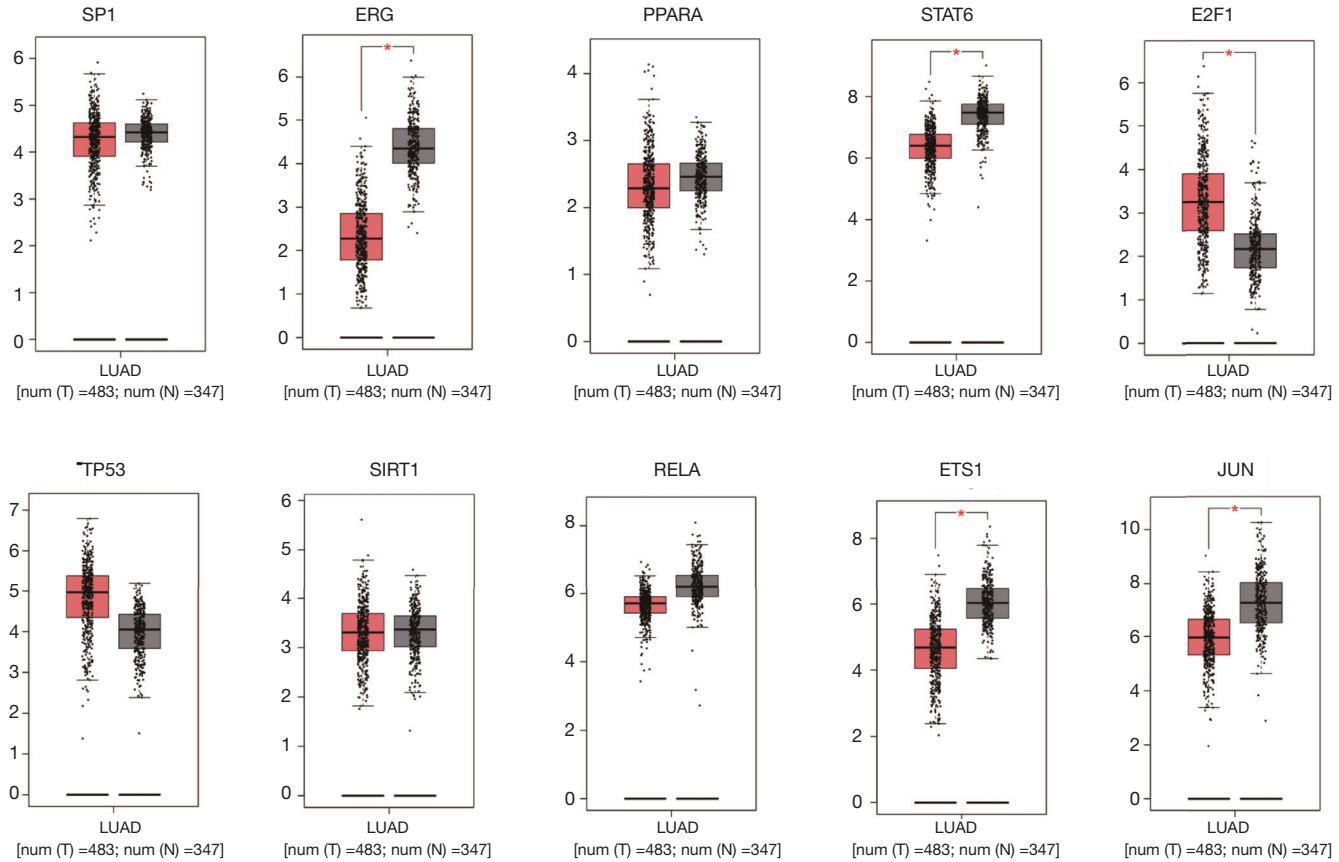

Figure 8 The expression of top 10 key TFs in GEPIA datasets. The red bars represent tumor samples, the gray bars represent normal samples and the red asterisk means a significant differential expression.

function annotation, pathways enrichment and PPI network analysis on the DEGs. For the downregulated DEGs, pathway enrichment analysis revealed that the extracellular matrix organization was significantly enriched, which was essential on the development and progression of cancers (27,28). In progression of cancer, the extracellular matrix becomes aligned and providing "highways" for accelerate tumor cell invasion (27,29,30). For the upregulated DEGs, pathway enrichment analysis revealed that Cell cycle mitotic was significantly enriched. DNA replicated and generated two identical copies of each chromosome during the cell cycle, and then two chromosomes segregated evenly to the two daughter cells. Cells would lose genomic stability and become malignant if receive chromosomes not evenly (31,32). Factors regulating the cell cycle mitotic play an important role in the occurrence and progress of tumors (33).

Many studies have revealed that both TFs and miRNAs play critical roles in the regulation of mRNAs and participate in the pathogenesis of cancer. Therefore, TF-gene-miRNA regulate network construction is essential for exploring the molecular mechanism of LUAD. First, the targets TF and miRNA were predicted based on these DEGs. Then, a TF-gene-miRNA co-expression network of LUAD was constructed to identify hub genes, TFs and miRNAs by Cytoscape. In total, 10 hub genes, 10 key miRNAs and 10 key TFs were located in the central hub of the TF-gene-miRNA co-expression network. GEPIA was used to verify the differential expressions of these key nodes in the LUAD patients. We found that 9 genes, 5 TFs and 6 miRNAs were differential expressed in LUAD. In addition, survival analysis of these key genes, TFs and miRNAs were performed by using the Kaplan-Meier Plotter analysis website. As a result, a total of 7 key genes, 4 key TFs and 2 key miRNAs with significance were finally obtained.

Herein, we found seven key genes, including *PHACTR2*, *MSRB3*, *GHR*, *PLSCR4*, *EPB41L2*, *NPNT* and *FBXO32*, were significantly associated with the prognosis of LUAD. These genes may contribute to the progression of LUAD

© Journal of Thoracic Disease. All rights reserved.

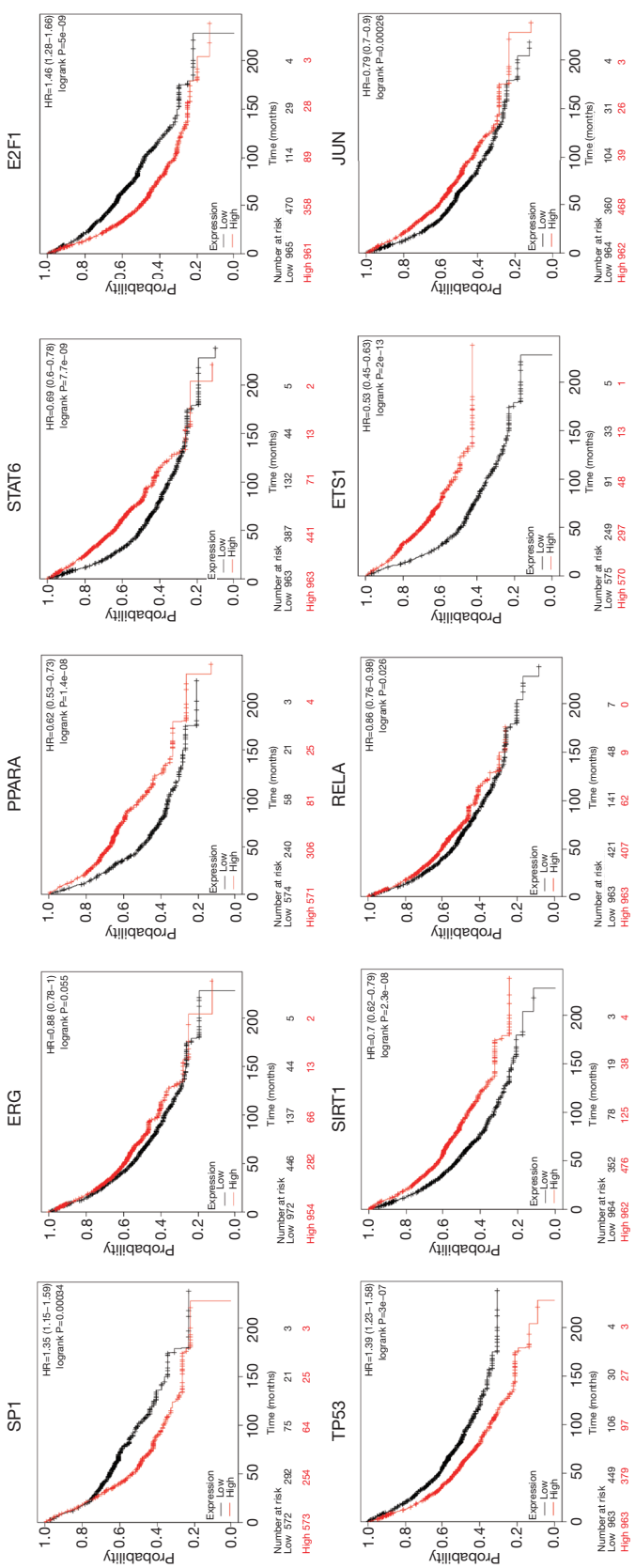

Figure 9 The prognosis value of 10 key TFs in the Kaplan-Meier Plotter analysis. The red lines represent high expression samples, the black lines represent low expression samples.

© Journal of Thoracic Disease. All rights reserved.

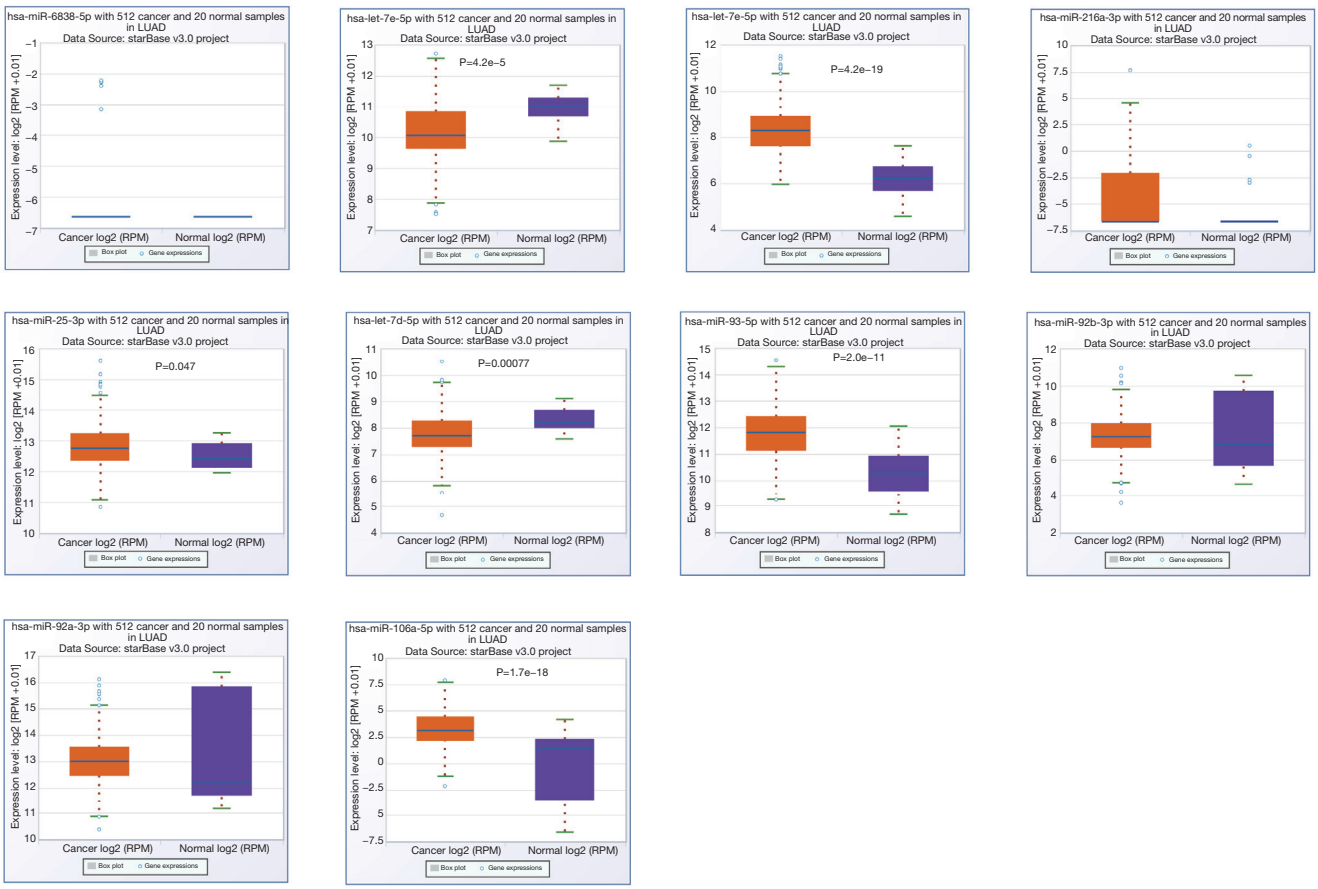

Figure 10 The expression of top 10 key miRNAs in starBase datasets. The yellow bars represent tumor samples and the blue bars represent normal samples.

and could be regarded as biomarkers and therapeutic targets of LUAD. MSRB3 plays an important role in cancer cell apoptosis through ROS production and endoplasmic reticulum stress status (34,35). Morel *et al.* found that MSRB3 maintain the genome stability of breast cancer (36). Ma *et al.* also reported that high MSRB3 expression was related with poor prognosis in gastric cancer (37). FBXO32 (also known as atrogin-1) is a member of the F-box protein family and an upstream regulator of epithelial-mesenchymal transition (EMT), which promotes EMT during tumor metastasis (38). FBXO32, as a TGF-β/Smad target gene, had shown biological activities in cell survival, and involved in several kinds of tumors including esophageal squamous cell carcinoma (39), pancreatic cancer (40) and colorectal cancer (41). Nephronectin (NPNT), an extracellular matrix protein, plays a major role in epithelial-mesenchymal interactions and signal transduction. Wang D *et al.* found that NPNT was a critical regulator of breast cancer metastases, which can promoted bone metastases in the early-stage of breast cancer by regulating the osteogenic niche (42) PHACTR2 (phosphatase and actin regulator 2) was found to be a novel genetic biomarker of cellular DNA repair in lung cancer by a GWAS study (43). PLSCR4 (phospholipid scramblase 4) is a member of transmembrane proteins family localized at the plasma membrane and often stimulated by proinflammatory cytokines. The diverse roles of PLSCRs in multiple cellular processes including immuno-activation, tumorigenesis, cell apoptosis and proliferation have been revealed by recent studies (44,45). Pienkowska *et al.* reported that PLSCR4 was identified as potential biomarkers for choroid plexus tumor aggressiveness in a DNA methylation profiles study (46). However, to the best of our knowledge, the function of PLSCR4 had not been well studied so far. Our study was the first time to report PLSCR4 as a key gene was associated with LUAD and may be a potential biomarker or

© Journal of Thoracic Disease. All rights reserved.

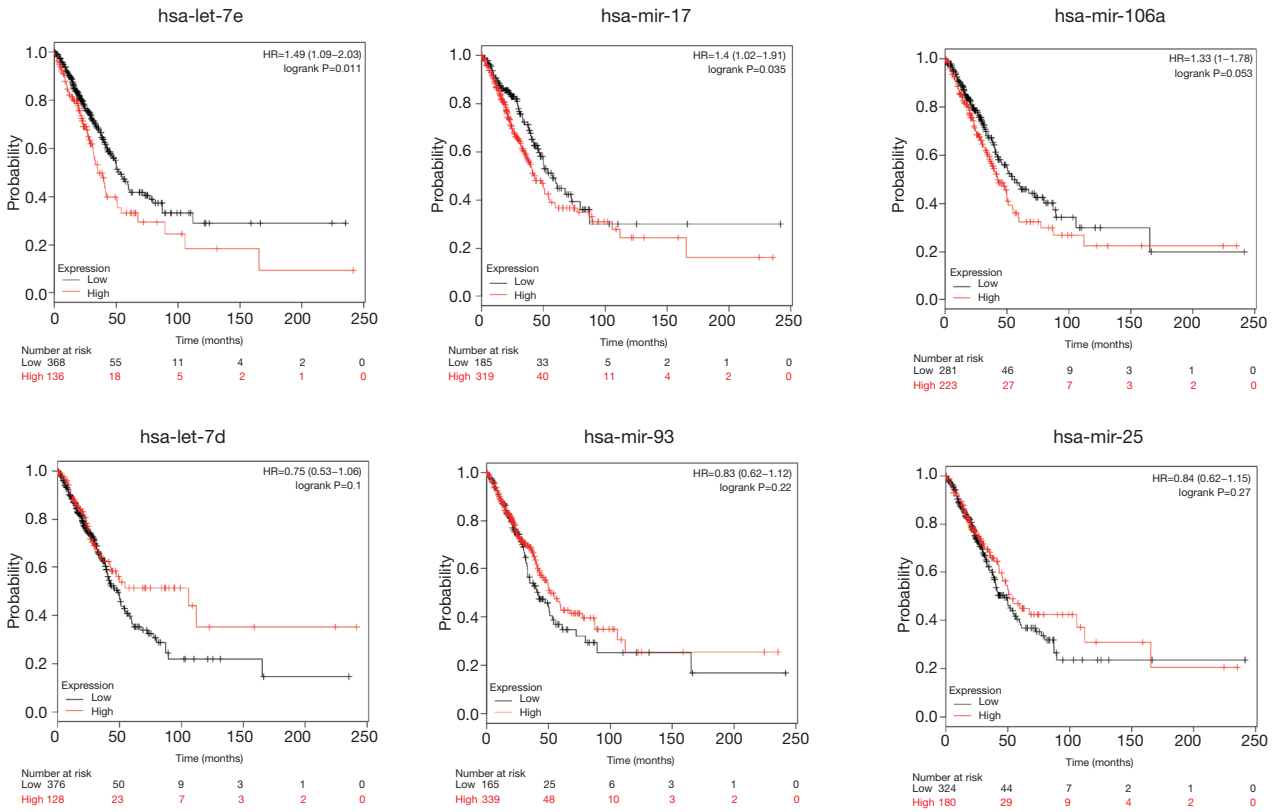

Figure 11 The prognosis value of 10 key miRNAs (only six miRNAs show useful data) in the Kaplan-Meier Plotter analysis. The red lines represent high expression samples, the black lines represent low expression samples.

therapy target of LUAD.

In addition, four key TFs (TAT6, E2F1, ETS1 and JUN) and two key miRNAs (hsa-let-7e-5p and hsa-miR-17-5p) were also significantly associated with the prognosis of LUAD. According to recent studies, all these 4 TFs have been verified as key regulators and potential therapy targets of numerous cancers including LUAD (47,48). Moreover, Chen *et al.* found that hsa-let-7e-5p could stimulate colorectal cancer cell migration and was a potential prognosis marker for rectal carcinoma with liver metastases (49). Hsa-let-7e-5p was over-expressed in head and neck squamous cell carcinoma cells (HNSCC) ,which would inhibit the proliferation and metastasis of HNSCC by inhibiting the expression of chemokine receptor 7 (50). Hsa-miR-17-5p was identified as a dominating oncogenic miRNA by downregulating tumor suppressors in a large pan-cancer research, including 15 epithelial cancer types and 7316 clinical samples (51). Hsa-miR-17-5p was also identified have a significant association with brain metastases breast cancer by bioinformatic analysis of GEO database (52). Shukla *et al.* reported that hsa-miR-17-5p was upregulated in serum and tissue of 115 cervical cancer patients and may become a potential biomarker as a biosignature of clinical relevance (53). Zhang *et al.* reported that circulating exosomal miR-17-5p was significantly upregulated in NSCLC patients and was a promising novel clinical diagnostic marker in the diagnosis of NSCLC (54).

In order to explore potential pathways between miRNA-gene-TF, we analyzed the co-expression relationship of miRNA-gene and TF-gene. The result revealed that hsa-miR-17-5p and PLSCR4 had a significant negative co-expression relationship in LUAD by miRNA/gene co-expression analysis. Further, we predicted that hsa-miR-17-5p have a binding site with PLSCR4 by using starBase website tool, which revealed that hsa-miR-17-5p may bind to PLSCR4 and inhibit the expression of PLSCR4. In the present study, PLSCR4 was identified as a downregulated DEG in LUAD. Recent study also suggested that the level of miR-17-5p was significantly higher in LUAD compared with healthy control subjects (54). Taken together, these

© Journal of Thoracic Disease. All rights reserved.

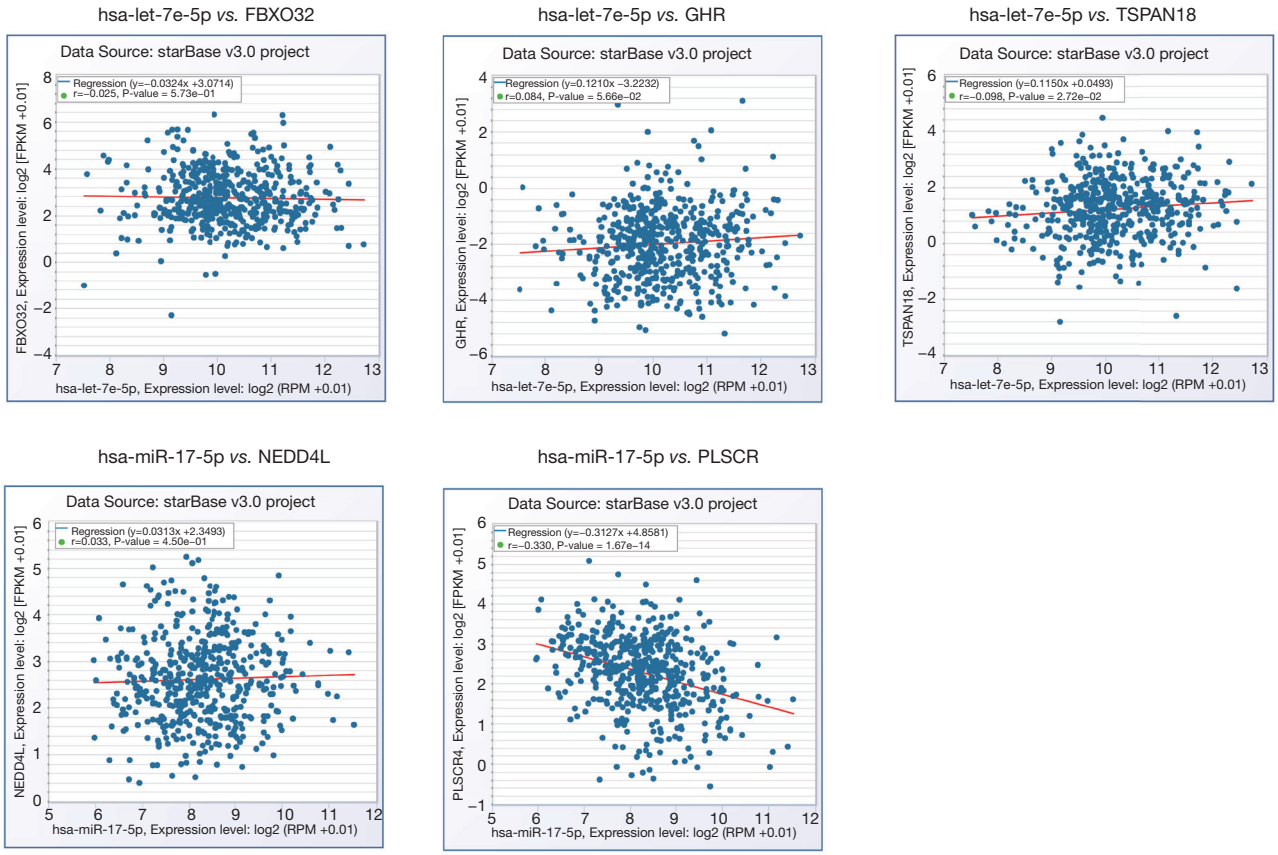

Figure 12 The co-expression between key miRNAs and genes in LUAD predicted by starBase. LUAD, lung adenocarcinoma.

findings suggested that hsa-miR-17-5p and its target gene PLSCR4 may play an important role in LUAD. The relationship between hsa-miR-17-5p and PLSCR4 has not been reported so far. Our study was the first time to report the co-expression relationship between hsa-miR-17-5p and PLSCR4. But the result was based on bioinformatics, and biological experiment *in vivo* and *vitro* would perform to further validate the result.

Conclusions

In our study, we finally identified seven key genes (*PHACTR2*, *MSRB3*, *GHR*, *PLSCR4*, *EPB41L2*, *NPNT*, *FBXO32*), two key miRNAs (hsa-let-7e-5p, hsa-miR-17-5p) and four key TFs (STAT6, E2F1, ETS1, JUN) as key factors of LUAD by integrating the data of GEO and TCGA database and constructing the TF-gene-miRNA co-expression network. Furthermore, the present study also found that hsa-miR-17-5p and its target gene PLSCR4 may play an important role in LUAD. The findings may provide further understanding of the pathogenesis of LUAD and provide novel insights for the diagnosis and treatment of LUAD. However, there are still the limitations in this study. Our results were based on public database and bioinformatics analysis, a clinical study of large samples and biological experiment would perform in the future to further validate the results.

Acknowledgments

Funding: This work was supported by grants from the National Natural Science Foundation of China (81573234 and 81773445) and "333"Project Of Jiangsu Province (LGY2016006).

Footnote

Conflicts of Interest: All authors have completed the ICMJE uniform disclosure form (available at http://dx.doi.org/10.21037/jtd-19-4168). The authors have no conflicts of

© Journal of Thoracic Disease. All rights reserved.

interest to declare.

Ethical Statement: The authors are accountable for all aspects of the work in ensuring that questions related to the accuracy or integrity of any part of the work are appropriately investigated and resolved.

Open Access Statement: This is an Open Access article distributed in accordance with the Creative Commons Attribution-NonCommercial-NoDerivs 4.0 International License (CC BY-NC-ND 4.0), which permits the non-commercial replication and distribution of the article with the strict proviso that no changes or edits are made and the original work is properly cited (including links to both the formal publication through the relevant DOI and the license). See: https://creativecommons.org/licenses/by-nc-nd/4.0/.

References

1. Torre LA, Bray F, Siegel RL, et al. Global cancer statistics, 2012. CA Cancer J Clin 2015;65:87-108.
2. DeSantis CE, Siegel RL, Sauer AG, et al. Cancer statistics for African Americans, 2016: Progress and opportunities in reducing racial disparities. CA Cancer J Clin 2016;66:290-308.
3. Rudin CM, Poirier JT, Byers LA, et al. Molecular subtypes of small cell lung cancer: a synthesis of human and mouse model data. Nat Rev Cancer 2019;19:289-97.
4. Moses MA, George AL, Sakakibara N, et al. Molecular Mechanisms of p63-Mediated Squamous Cancer Pathogenesis. Int J Mol Sci 2019;20:3590.
5. Li Y, Chen Y, Li J, et al. Co-delivery of microRNA-21 antisense oligonucleotides and gemcitabine using nanomedicine for pancreatic cancer therapy. Cancer Sci 2017;108:1493-503.
6. Cheng CJ, Bahal R, Babar IA, et al. MicroRNA silencing for cancer therapy targeted to the tumour microenvironment. Nature 2015;518:107-10.
7. Rupaimoole R, Slack FJ. MicroRNA therapeutics: towards a new era for the management of cancer and other diseases. Nat Rev Drug Discov 2017;16:203-22.
8. Bhayadia R, Krowiorz K, Haetscher N, et al. Endogenous Tumor Suppressor microRNA-193b: Therapeutic and Prognostic Value in Acute Myeloid Leukemia. J Clin Oncol 2018;36:1007-16.
9. Zeng JH, Xiong DD, Pang YY, et al. Identification of molecular targets for esophageal carcinoma diagnosis using miRNA-seq and RNA-seq data from The Cancer Genome Atlas: a study of 187 cases. Oncotarget 2017;8:35681-99.
10. Chen B, Gao S, Ji C, et al. Integrated analysis reveals candidate genes and transcription factors in lung adenocarcinoma. Mol Med Rep 2017;16:8371-9.
11. Kabbout M, Garcia MM, Fujimoto J, et al. ETS2 mediated tumor suppressive function and MET oncogene inhibition in human non-small cell lung cancer. Clin Cancer Res 2013;19:3383-95.
12. Marwitz S, Depner S, Dvornikov D, et al. Downregulation of the TGFbeta Pseudoreceptor BAMBI in Non-Small Cell Lung Cancer Enhances TGFbeta Signaling and Invasion. Cancer Res 2016;76:3785-801.
13. Selamat SA, Chung BS, Girard L, et al. Genome-scale analysis of DNA methylation in lung adenocarcinoma and integration with mRNA expression. Genome Res 2012;22:1197-211.
14. Smoot ME, Ono K, Ruscheinski J, et al. Cytoscape 2.8: new features for data integration and network visualization. Bioinformatics 2011;27:431-2.
15. Szklarczyk D, Franceschini A, Wyder S, et al. STRING v10: protein–protein interaction networks, integrated over the tree of life. Nucleic Acids Res 2015;43:D447.
16. Dweep H, Gretz N. miRWalk2.0: a comprehensive atlas of microRNA-target interactions. Nat Methods 2015;12:697.
17. Han H, Cho JW, Lee S, et al. TRRUST v2: an expanded reference database of human and mouse transcriptional regulatory interactions. Nucleic Acids Res 2018;46:D380-D386.
18. Tang Z, Li C, Kang B, et al. GEPIA: a web server for cancer and normal gene expression profiling and interactive analyses. Nucleic Acids Res 2017;45:W98-W102.
19. Gy rffy B, Surowiak P, Budczies J, et al. Online Survival Analysis Software to Assess the Prognostic Value of Biomarkers Using Transcriptomic Data in Non-Small-Cell Lung Cancer. Plos One 2013;8:e82241.
20. Li JH, Liu S, Zhou H, et al. starBase v2.0: decoding miRNA-ceRNA, miRNA-ncRNA and protein-RNA interaction networks from large-scale CLIP-Seq data. Nucleic Acids Res 2014;42:D92-7.
21. Politi K, Herbst RS. Lung cancer in the era of precision medicine. Clin Cancer Res 2015;21:2213-20.
22. Herbst RS, Morgensztern D, Boshoff C. The biology and management of non-small cell lung cancer. Nature 2018;553:446-54.
23. Blons H, Garinet S, Laurent-Puig P, et al. Molecular markers and prediction of response to immunotherapy in non-small cell lung cancer, an update. J Thorac Dis 2019;11:S25-S36.

© Journal of Thoracic Disease. All rights reserved.

24. Brognard J, Clark AS, Ni Y, et al. Akt/protein kinase B is constitutively active in non-small cell lung cancer cells and promotes cellular survival and resistance to chemotherapy and radiation. Cancer Res 2001;61:3986-97.
25. Song Z, Yu X, Zhang Y. Mutation and prognostic analyses of PIK3CA in patients with completely resected lung adenocarcinoma. Cancer Med 2016;5:2694-700.
26. Singh SS, Dahal A, Shrestha L, et al. Genotype Driven Therapy for Non-Small Cell Lung Cancer: Resistance, Pan Inhibitors and Immunotherapy. Curr Med Chem 2019. [Epub ahead of print].
27. Pickup MW, Mouw JK, Weaver VM. The extracellular matrix modulates the hallmarks of cancer. EMBO reports 2014;15:1243-53.
28. Lee S, Han H, Koo H, et al. Extracellular matrix remodeling in vivo for enhancing tumor-targeting efficiency of nanoparticle drug carriers using the pulsed high intensity focused ultrasound. J Control Release 2017;263:68-78.
29. Jones CE, Hammer AM, Cho Y, et al. Stromal PTEN Regulates Extracellular Matrix Organization in the Mammary Gland. Neoplasia 2019;21:132-45.
30. Stevens LE, Cheung WKC, Adua SJ, et al. Extracellular Matrix Receptor Expression in Subtypes of Lung Adenocarcinoma Potentiates Outgrowth of Micrometastases. Cancer Res 2017;77:1905-17.
31. Schvartzman JM, Sotillo R, Benezra R. Mitotic chromosomal instability and cancer: mouse modelling of the human disease. Nat Rev Cancer 2010;10:102-15.
32. Solomon DA, Kim T, Diaz-Martinez LA, et al. Mutational inactivation of STAG2 causes aneuploidy in human cancer. Science 2011;333:1039-43.
33. Thole TM, Lodrini M, Fabian J, et al. Neuroblastoma cells depend on HDAC11 for mitotic cell cycle progression and survival. Cell Death Dis 2017;8:e2635.
34. Kwak GH, Kim HY. MsrB3 deficiency induces cancer cell apoptosis through p53-independent and ER stress-dependent pathways. Arch Biochem Biophys 2017;621:1-5.
35. Kwak GH, Kim TH, Kim HY. Down-regulation of MsrB3 induces cancer cell apoptosis through reactive oxygen species production and intrinsic mitochondrial pathway activation. Biochem Biophys Res Commun 2017;483:468-74.
36. Morel AP, Ginestier C, Pommier RM, et al. A stemness-related ZEB1-MSRB3 axis governs cellular pliancy and breast cancer genome stability. Nat Med 2017;23:568-78.
37. Ma X, Wang J, Zhao M, et al. Increased expression of methionine sulfoxide reductases B3 is associated with poor prognosis in gastric cancer. Oncol Lett 2019;18:465-71.
38. Sahu SK, Tiwari N, Pataskar A, et al. FBXO32 promotes microenvironment underlying epithelial-mesenchymal transition via CtBP1 during tumour metastasis and brain development. Nat Commun 2017;8:1523.
39. Guo W, Zhang M, Shen S, et al. Aberrant methylation and decreased expression of the TGF- /Smad target gene FBXO32 in esophageal squamous cell carcinoma. Cancer 2014;120:2412-23.
40. Yang C, Fan P, Zhu S, et al. 3F-Box protein 32 degrades ataxia telangiectasia and Rad3-related and regulates DNA damage response induced by gemcitabine in pancreatic cancer. Oncol Lett 2018;15:8878-84.
41. Yuan X, Zhang Z, Jiang K, et al. Preliminary Study of the Role F-Box Protein 32 (FBXO32) in Colorectal Neoplasms Through the Transforming Growth Factor beta (TGF-)/Smad4 Signalling Pathway. Med Sci Monit 2018;24:1080-8.
42. Wang D, Zhao C, Gao L, et al. NPNT promotes early-stage bone metastases in breast cancer by regulation of the osteogenic niche. J Bone Oncol 2018;13:91-6.
43. Wang LE, Gorlova OY, Ying J, et al. Genome-wide association study reveals novel genetic determinants of DNA repair capacity in lung cancer. Cancer Res 2013;73:256-64.
44. Kodigepalli KM, Bowers K, Sharp A, et al.. Roles and regulation of phospholipid scramblases. FEBS Lett 2015;589:3-14.
45. Mutch DM, O'Maille G, Wikoff WR, et al. Mobilization of pro-inflammatory lipids in obese Plscr3-deficient mice. Genome Biol 2007;8:R38.
46. Pienkowska M, Choufani S, Turinsky AL, et al. DNA methylation signature is prognostic of choroid plexus tumor aggressiveness. Clin Epigenetics 2019;11:117.
47. Shanmugam MK, Lee JH, Chai EZ, et al. Cancer prevention and therapy through the modulation of transcription factors by bioactive natural compounds. Semin Cancer Biol 2016;40-41:35-47 .
48. Rajagopal C, Lankadasari MB, Aranjani JM, et al. Targeting oncogenic transcription factors by polyphenols: A novel approach for cancer therapy. Pharmacol Res 2018;130:273-91.
49. Chen W, Lin G, Yao Y et al. MicroRNA hsa-let-7e-5p as a potential prognosis marker for rectal carcinoma with liver metastases. Oncol Lett 2018;15:6913-24.
50. Wang S, Jin S, Liu MD, et al. Hsa-let-7e-5p Inhibits the Proliferation and Metastasis of Head and Neck Squamous

© Journal of Thoracic Disease. All rights reserved.

Cell Carcinoma Cells by Targeting Chemokine Receptor 7. J Cancer 2019;10:1941-8.
51. Dhawan A, Scott JG, Harris AL, et al. Pan-cancer characterisation of microRNA across cancer hallmarks reveals microRNA-mediated downregulation of tumour suppressors. Nat Commun 2018;9:5228.
52. Li Z, Peng Z, Gu S, et al. Global Analysis of miRNA-mRNA Interaction Network in Breast Cancer with Brain Metastasis. Anticancer Res 2017;37:4455-68.
53. Shukla V, Varghese VK, Kabekkodu SP, et al. Enumeration of deregulated miRNAs in liquid and tissue biopsies of cervical cancer. Gynecol Oncol 2019;155:135-43.
54. Zhang Y, Zhang Y, Yin Y, et al. Detection of circulating exosomal miR-17-5p serves as a novel non-invasive diagnostic marker for non-small cell lung cancer patients. Pathol Res Pract 2019;215:152466.

Cite this article as: Li J, Li Z, Zhao S, Song Y, Si L, Wang X. Identification key genes, key miRNAs and key transcription factors of lung adenocarcinoma. J Thorac Dis 2020;12(5):1917-1933. doi: 10.21037/jtd-19-4168

© Journal of Thoracic Disease. All rights reserved.

Supplementary

Table S1 Overlapped downregulated genes

Genes
FABP4
SLC6A4
WIF1
TMEM100
AGER
GKN2
ANKRD1
RTKN2
SOST/DCT
SFTPC
FCN3
FHL1
ADH1B
EDNRB
TEK
ACADL
LYSE1
CPB2
CLIC5
SCGB1A1
AQP4
CYP4B1
EMCN
MME
FMO2
CLDN18
ABCA8
PEBP4
HHIP
HBB
SEMA6A
PTPRB
MAMDC2
CAV1
SDPR
CRYAB
CD36
GPC3
TGFBR3
PGC
ANKRD29
HSD17B6
MT1M
CALCRL
GNG11
PDK4
STABP6
FAM189A2
COL6A6
CDH5
SLC19A3
EDN1
VIPR1
STX11
NOSTRIN
LRRN3
MFAP4
CACNA1D2
TSPAN7
HIG1B
TCF21
IL33
MS4A15
SLIT2
KLF4
ABI3BP
ITLN2
LFL
CDHR3
LDB2
BCHE
HSPB8
MMRN1
TNNC1
JAM2
VWF
SPOCK2
PLAC8
SEMA5A
AADAC
CYYR1
FOSB
EPAS1
NPNT
DACH1
SLC39A8
LAMP3
C10orf67
FGFBP2
TMOD1
GPM6
PLAC1/8
AOC3
TMEM47
RHOJ
GHR
HEG1
GIMAP8
CDH13
AFF3
LRRK2
GLDN
FDZD2
SASH1
FRG4
ANGPT1
S100A1
ANXA3
PECAM1
ZBTB16
SUSD2
C7
PDE5A
LHFP
OLR1
HPSE
KIAA1324L
CGNL1
SPARCL1
ACVRL1
EML1
FLRT3
C20orf85
CYBRD1
VGLL3
ABCA3
CTNNAL1
BSGAL/NT1
SLC0DA1
CLEC1A
ADH1A
FAM107A
LIMCH1
ITM2A
CSRNP1
DUOX1
PAPSS2
ADAMTS1
CD93
FPR2
FZD4
NDNF
RAMP2
SIRPX
CLEC14A
PROS1
NEDD9
DES
DPT
RGRN/1L
MAOB
DMBT1
ADH1
FGD5
CES1
LRRC32
STARD13
CXCR7
TSPAN18
ID1
PTRF
TPPP3
RNF144B
FBLN5
CRTAC1
MSRB3
HEY1
GSTM5
SLIT3
SFTPD
C1orf198
MYH10
SLPI
PGM5
DPYSL2
OLFML1
CDO1
FERMT2
GLIPR2
PPP1R14A
PROCKLE2
SGCE
C3orf40
CLEC3B
SOCS2
FEZ1
ARHGEF6
GPM6B
REN2
ESAM
VSIG4
GBP4
FRAS1
SPTBN1
TACC1
FOS
EFEMP1
C4A
SESN1
MAOA
MAMCD
HOXA5
METTL7A
PCDLCZ3
ARHGAP44
IL7R
RRAS
ICAM2
ACTG2
MSR1
GIMAP7
S100A3
SELE
NDRG4
PTPN4
PLSCR4
EPB41L2
LGI3
STARD8
CAT
IRAS/F3
RAMP3
CPA3
ADAMB1
ZNF385B
FMO3
TBX3
TMEM204
NDRG2
SMAD6
C9B
PDLIM3
DCN
EMP1
TGFBR2
MYL9
AGR3
WFS1
LDLR
CHSLZ
CA2
C1orf87
NTN4
NEDD4L
LMCD1
PHACTR2
TIMP3
GIMAP4
DUSP1
SELENBP1
SERPY1
C4BPA
PID1
CBX7
MYADM
KLF6
CD34
ADCY4
MS4A2
AJM
ZFP36
FAM155B

Table S2 Overlapped upregulated genes

Genes
NRK2
AURKA
SPDEF
SLC35F2
FLPC2
GLB1L2
EPG5HK
METTL7B
FUT3
CLDN10
SERINC2
CDC45
DSP
LAD1
RPL39L
SLC50A1
SLC7A5
KDELR3
ECT2
TIAM2
ETV4
CHRNA5
CDC20
IL37
PYCR1
TNFRSF21
SMPDL3B
MELK
CJB2
PRDM2
IGF2BP3
ATP10B
PRC1
SFN
FBXO32
STIL
FUT2
CDCA7
TFAP2A
KIF25A
CTHRC1
HMGB3
CCNB2
FGAT1
AIM2
KIAA0101
MMP9
SULF1
PCPH
COL3A1
C15orf48
OCIAD2
NQO1
GOLM1
MUC21
MMP11
THBS2
COL10A1
ASPM
GCNT3
FAM83A
TPX2
UBE2T
CENPF
SLC4A1
CRABP2
CDH3
COL1A1
TOP2A
ANKRD22
CEACAM5
MMP12
TMPRSS4
SPINK1
SPP1

Table S3 String interactions

Node 1	Node 2	node1_string_internal_id	node2_string_internal_id	node1_external_id	node2_external_id	neighborhood_on_chromosome	gene_fusion	phylogenetic_cooccurrence	Homology	Coexpression	experimentally_determined_interaction	database_annotated	automated_textmining	combined_score
CDC20	NEK2	4443940	4442784	9606.ENSP00000361540	9606.ENSP00000355966	0	0	0	0	0.948	0.993	0.9	0.81	0.999
ANGPT1	TEK	4449446	4445310	9606.ENSP00000428340	9606.ENSP00000369375	0	0	0	0	0.076	0.385	0.9	0.986	0.999
CDC20	AURKA	4443940	4432988	9606.ENSP00000361540	9606.ENSP00000216911	0	0	0	0	0.977	0.379	0.9	0.743	0.999
CCNB2	AURKA	4436767	4432988	9606.ENSP00000288207	9606.ENSP00000216911	0	0	0	0	0.973	0.896	0	0.696	0.999
EDN1	EDNRB	4445200	4444853	9606.ENSP00000368683	9606.ENSP00000366416	0	0	0	0	0	0.951	0.9	0.964	0.999
CDC20	CCNB2	4443940	4436767	9606.ENSP00000361540	9606.ENSP00000288207	0	0	0	0	0.989	0.71	0.9	0.829	0.999
TPX2	AURKA	4437665	4432988	9606.ENSP00000300403	9606.ENSP00000216911	0	0	0	0	0.952	0.982	0.9	0.886	0.999
CALCRL	RAMP2	4447454	4434325	9606.ENSP00000386972	9606.ENSP00000253796	0	0	0	0	0.063	0.852	0.9	0.955	0.999
TOP2A	TPX2	4448614	4437665	9606.ENSP00000411532	9606.ENSP00000300403	0	0	0	0	0.993	0	0	0.595	0.997
CALCRL	RAMP3	4447454	4433813	9606.ENSP00000386972	9606.ENSP00000242249	0	0	0	0	0.061	0.379	0.9	0.952	0.996
CENPF	CCNB2	4442771	4436767	9606.ENSP00000355922	9606.ENSP00000288207	0	0	0	0	0.901	0	0.9	0.544	0.995
KIF20A	PRC1	4446341	4446249	9606.ENSP00000378356	9606.ENSP00000377793	0	0	0	0	0.892	0.182	0.9	0.468	0.994
COL3A1	COL1A1	4438049	4433346	9606.ENSP00000304408	9606.ENSP00000225964	0	0	0.439	0.951	0.944	0	0.9	0.901	0.994
NEK2	TPX2	4442784	4437665	9606.ENSP00000355966	9606.ENSP00000300403	0	0	0	0	0.868	0	0.9	0.543	0.993
CDC20	CENPF	4443940	4442771	9606.ENSP00000361540	9606.ENSP00000355922	0	0	0	0	0.839	0	0.9	0.596	0.992
NEK2	AURKA	4442784	4432988	9606.ENSP00000355966	9606.ENSP00000216911	0	0	0.361	0.69	0.877	0	0.9	0.679	0.99
SFTPD	DMBT1	4443913	4443222	9606.ENSP00000361366	9606.ENSP00000357905	0	0	0	0	0.063	0.379	0.9	0.819	0.988
PECAM1	CDH5	4450567	4441389	9606.ENSP00000457421	9606.ENSP00000344115	0	0	0	0	0.143	0	0.8	0.938	0.988
TOP2A	CCNB2	4448614	4436767	9606.ENSP00000411532	9606.ENSP00000288207	0	0	0	0	0.965	0.057	0	0.623	0.986
TOP2A	CDC20	4448614	4443940	9606.ENSP00000411532	9606.ENSP00000361540	0	0	0	0	0.968	0	0	0.579	0.986
PRC1	TPX2	4446249	4437665	9606.ENSP00000377793	9606.ENSP00000300403	0	0	0	0	0.966	0	0	0.577	0.985
PRC1	CDC20	4446249	4443940	9606.ENSP00000377793	9606.ENSP00000361540	0	0	0	0	0.967	0	0	0.56	0.985
SFTPD	SFTPC	4443913	4439043	9606.ENSP00000361366	9606.ENSP00000316152	0	0	0	0	0.334	0	0.9	0.8	0.985

Table S4 Mcc top 20 genes

Rank	Name	Score
1	*AURKA*	1.44E+09
2	*ASPM*	1.44E+09
2	*MELK*	1.44E+09
2	*TPX2*	1.44E+09
2	*TOP2A*	1.44E+09
2	*CENPF*	1.44E+09
7	*CDC20*	1.44E+09
8	*CCNB2*	1.44E+09
9	*KIAA0101*	1.44E+09
9	*KIF20A*	1.44E+09
11	*PRC1*	1.44E+09
12	*CDC45*	9.62E+08
13	*NEK2*	9.58E+08
14	*TYMS*	4.83E+08
15	*ECT2*	4.79E+08
16	*UBE2T*	3,628,800
17	*STIL*	5,040
18	*GNG11*	176
19	*ADCY4*	151
20	*VIPR1*	120

Top 20 in network string_interactions (1).tsv ranked by MCC method.

| | | |

MCODE App Results

Date: 2019-7-19 11:53:22

Parameters:

Network Scoring:

Include Loops: false Degree Cutoff: 2

Cluster Finding:

Node Score Cutoff: 0.2 Haircut: true Fluff: false K-Core: 2 Max. Depth from Seed: 100

Cluster	Score (Density*#Nodes)	Nodes	Edges	Node IDs
1	14.933	16	112	AURKA, MELK, NEK2, ECT2, CDC20, CDC45, TYMS, PRC1, KIF20A, CENPF, KIAA0101, TOP2A, ASPM, TPX2, UBE2T, CCNB2
2	5.4	11	27	RAMP3, ADCY4, S1PR1, CX3CR1, RAMP2, CALCRL, VIPR1, GNG11, GRK5, EDNRB, EDN1
3	5	5	10	GOLM1, GPC3, WFS1, SPP1, SPARCL1
4	4.5	9	18	CD36, CDH5, VWF, PECAM1, TEK, CD34, CD93, PTPRB, OLR1
5	4.5	5	9	MAOA, MAOB, AOX1, ADH1A, ADH1B
6	4	4	6	FBXO32, RNF144B, NEDD4L, ZBTB16
7	4	4	6	COL1A1, COL3A1, COL10A1, COL6A6
8	4	4	6	DUSP1, FOSB, FOS, ZFP36
9	3	3	3	PROS1, A2M, MMRN1
10	3	3	3	FZD4, LDLR, IL7R
11	3	3	3	THBS2, SEMA5A, ADAMTS1
12	2.75	9	11	FBLN5, MFAP4, SCGB1A1, CLEC3B, SEPP1, SFTPD, SFTPC, TIMP3, EFEMP1

Figure S1 Mcode of PPI network. PPI, protein-protein interaction.

Table S6 Target TFs of DEGs

TF	Gene	P
SP1	*ACVRL1*	2.41E-06
SP1	*MMRN1*	2.41E-06
SP1	*CDH3*	2.41E-06
SP1	*EDNRB*	2.41E-06
SP1	*WIF1*	2.41E-06
SP1	*SLC19A3*	2.41E-06
SP1	*TGFBR2*	2.41E-06
SP1	*MME*	2.41E-06
SP1	*TYMS*	2.41E-06
SP1	*SLC39A8*	2.41E-06
SP1	*CES1*	2.41E-06
SP1	*MMP9*	2.41E-06
SP1	*TIMP3*	2.41E-06
SP1	*MAOB*	2.41E-06
SP1	*MMP11*	2.41E-06
SP1	*SLC7A5*	2.41E-06
SP1	*CAT*	2.41E-06
SP1	*DPYSL2*	2.41E-06
SP1	*SPP1*	2.41E-06
SP1	*COL1A1*	2.41E-06
SP1	*LPL*	2.41E-06
SP1	*FOS*	2.41E-06
SP1	*CAV1*	2.41E-06
SP1	*LDLR*	2.41E-06
ERG	*ADAMTS1*	5.43E-06
ERG	*SPP1*	5.43E-06
ERG	*ICAM2*	5.43E-06
ERG	*VWF*	5.43E-06
ERG	*HPGD*	5.43E-06
ERG	*CDH5*	5.43E-06
PPARA	*LPL*	5.03E-05
PPARA	*ACADL*	5.03E-05
PPARA	*PDK4*	5.03E-05
PPARA	*MMP9*	5.03E-05
PPARA	*CD36*	5.03E-05
PPARA	*FABP4*	5.03E-05
GATA2	*PECAM1*	0.000273
GATA2	*ADH1A*	0.000273
GATA2	*MS4A2*	0.000273
GATA2	*DPYSL2*	0.000273
STAT6	*SELE*	0.000357
STAT6	*FOSB*	0.000357
STAT6	*FOS*	0.000357
STAT6	*COL1A1*	0.000357
STAT6	*DUSP1*	0.000357
TFCP2	*SPP1*	0.000394
TFCP2	*A2M*	0.000394
TFCP2	*TYMS*	0.000394
E2F1	*ETV4*	0.000527
E2F1	*MYH10*	0.000527
E2F1	*AURKA*	0.000527
E2F1	*CDCA7*	0.000527
E2F1	*PDK4*	0.000527
E2F1	*DUSP1*	0.000527
E2F1	*TYMS*	0.000527
E2F1	*TOP2A*	0.000527
E2F1	*ECT2*	0.000527
PPARD	*CAT*	0.000555
PPARD	*LPL*	0.000555
PPARD	*PDK4*	0.000555
TP53	*CCNB2*	0.000563
TP53	*CAV1*	0.000563
TP53	*TYMS*	0.000563
TP53	*SFN*	0.000563
TP53	*PRC1*	0.000563
TP53	*ID1*	0.000563
TP53	*SLC2A1*	0.000563
TP53	*DUSP1*	0.000563
TP53	*CRYAB*	0.000563
TP53	*ANKRD1*	0.000563
SIRT1	*TBX3*	0.00137
SIRT1	*COL10A1*	0.00137
SIRT1	*MMP9*	0.00137
SIRT1	*NQO1*	0.00137
SIRT1	*SELE*	0.00137
YBX1	*TOP2A*	0.00166
YBX1	*CDC20*	0.00166
YBX1	*TYMS*	0.00166
YBX1	*SLC6A4*	0.00166
RELA	*MMP9*	0.00225
RELA	*PDK4*	0.00225
RELA	*MMP12*	0.00225
RELA	*EDN1*	0.00225
RELA	*EPAS1*	0.00225
RELA	*GKN2*	0.00225
RELA	*COL1A1*	0.00225
RELA	*VWF*	0.00225
RELA	*EPCAM*	0.00225
RELA	*SELE*	0.00225
RELA	*LPL*	0.00225
RELA	*OLR1*	0.00225
ATF3	*SELE*	0.0024
ATF3	*LDLR*	0.0024
ATF3	*ID1*	0.0024
NFE2L2	*HBB*	0.0024
NFE2L2	*CAT*	0.0024
NFE2L2	*NQO1*	0.0024
ETS1	*TGFBR2*	0.00241
ETS1	*HPGD*	0.00241
ETS1	*TFAP2A*	0.00241
ETS1	*VWF*	0.00241
ETS1	*COL1A1*	0.00241
ETS1	*MMP9*	0.00241
JUN	*DCN*	0.00433
JUN	*MMP9*	0.00433
JUN	*EDN1*	0.00433
JUN	*HEY1*	0.00433
JUN	*NQO1*	0.00433
JUN	*MMP12*	0.00433
JUN	*CA2*	0.00433
JUN	*MSR1*	0.00433
RUNX1	*CD34*	0.00433
RUNX1	*KLF4*	0.00433
RUNX1	*MYL9*	0.00433
RUNX1	*MYH10*	0.00433
NR2F2	*TFAP2A*	0.00587
NR2F2	*HEY1*	0.00587
NFKB1	*EDN1*	0.00647
NFKB1	*PDK4*	0.00647
NFKB1	*GKN2*	0.00647
NFKB1	*SELE*	0.00647
NFKB1	*EPCAM*	0.00647
NFKB1	*MMP9*	0.00647
NFKB1	*AGER*	0.00647
NFKB1	*VWF*	0.00647
NFKB1	*LPL*	0.00647
NFKB1	*COL1A1*	0.00647
NFKB1	*A2M*	0.00647
NFKB1	*OLR1*	0.00647
HDAC1	*KLF4*	0.00756
HDAC1	*MMP9*	0.00756
HDAC1	*SPP1*	0.00756
HDAC1	*EPCAM*	0.00756
HDAC1	*FOS*	0.00756
HDAC5	*SLC2A1*	0.00773
HDAC5	*SLIT2*	0.00773
SRF	*MYL9*	0.00879
SRF	*MMP9*	0.00879
SRF	*FOS*	0.00879
SMAD4	*FBXO32*	0.00981
SMAD4	*DACH1*	0.00981
SMAD4	*ZFP36*	0.00981
ELF3	*MMP9*	0.00983
ELF3	*TIMP3*	0.00983
GATA6	*CAV1*	0.00983
GATA6	*VWF*	0.00983
HOXA9	*SELE*	0.00983
HOXA9	*CDH3*	0.00983
POU3F2	*CDH13*	0.00983
POU3F2	*PDE5A*	0.00983
SP2	*PAPSS2*	0.00983
SP2	*MMP9*	0.00983
PPARG	*KLF4*	0.000137
PPARG	*CD36*	0.000137
PPARG	*AGER*	0.000137
PPARG	*FABP4*	0.000137
PPARG	*CAV1*	0.000137
PPARG	*MMP9*	0.000137
PPARG	*CAT*	0.000137

Table **S7** The value of each nodes of T3 mdRNA gene network calculated by cytoHubba

node_name	MCC	MNC	Degree	EPC	BottleNeck	EcCentricity	Closeness	Radiality	Betweenness	Stress
NEDD4L	7	0	7	72	105.7	13	0.061	96.5	12.08	7009
LDLR	10	0	10	47	106.5	61	0.111	87.48	13.24	16585
PHACTR2	12	0	12	45	93.84	73	0.111	75.28	12.46	7093
MSRB3	5	0	5	42	20.32	7	0.077	38.9	8.591	3300
GHR	6	0	6	39	103.1	5	0.091	72.68	12.48	4382
rno-miR-6838-5p	9	0	9	32	105.6	31	0.083	79.8	12.78	8562
lsa-miR-7a-5p	7	0	7	30	103.1	25	0.083	74.85	12.42	6329
PLSCR4	7	0	7	30	106.2	19	0.091	75.51	12.51	7510
rno-miR-17-5p	6	0	6	27	106.4	14	0.1	77.39	12.81	9617
SP1	24	0	24	24	81.17	124	0.1	100.2	13.46	23313
rno-miR-218-5p	5	0	5	24	95.02	3	0.1	69.62	12.42	2551
rno-miR-25-3p	5	0	5	24	105.2	2	0.083	62.06	11.73	2667
TSPAN18	9	0	9	22	99.78	7	0.091	70.41	12.29	3033
EPB41L2	9	0	9	22	90.14	2	0.091	67.87	11.88	558
FBXO32	9	0	9	21	91.79	10	0.077	63.79	11.57	4247
NPY1R	3	0	3	21	103.8	2	0.091	52	9.9	1977
STARD13	7	0	7	20	103.6	8	0.091	68.32	12.23	2639
SULF1	4	0	4	20	81.94	3	0.091	57.79	11.47	1316
lsa-miR-7d-5p	7	0	7	18	102.1	3	0.1	68.32	12.56	1455
rno-miR-93-5p	5	0	5	18	105	4	0.1	70.09	12.41	2238
CACNA2D2	6	0	6	18	72.36	1	0.077	52.49	10.94	549.2
rno-miR-93b-3p	5	0	5	18	105	1	0.083	62.06	11.52	1011
rno-miR-92a-3p	4	0	4	17	103.1	2	0.083	55.06	11.14	1789
rno-miR-106a-5p	5	0	5	16	98.43	5	0.1	64.75	11.96	2293
rno-miR-130a-3p	4	0	4	16	103.8	1	0.083	55.06	11.14	2600
rno-miR-106-3p	3	0	3	16	93.06	2	0.071	60.25	11.67	1121
FZD4	13	0	13	15	95.02	13	0.091	82.17	13.72	4267
SPOCK2	5	0	5	15	88.7	5	0.077	47.63	10.18	2210
lsa-miR-7b-5p	5	0	5	15	101.2	1	0.083	67.19	11.99	953.8
rno-miR-20a-5p	5	0	5	15	104.4	1	0.1	72.36	12.56	2030
rno-miR-202-5p	2	0	2	15	20.25	3	0.071	33.74	7.669	1108
DPYSL2	8	0	8	14	96.66	7	0.091	81.55	13.02	5357
MME	4	0	4	14	21.04	4	0.091	60.25	12.48	1460
lsa-miR-7a-5p	3	0	3	13	101.6	1	0.083	67.88	12.06	1033
rno-miR-145-5p	3	0	3	13	87.1	1	0.083	57.79	11.47	2000
rno-miR-206-5p	5	0	5	13	101.9	18	0.1	70.56	13.43	1167
TACC1	2	0	2	13	96.42	3	0.077	62.97	11.97	1012
MMP9	12	0	12	12	65.48	11	0.111	83.59	13.07	1108
NPR3R	12	0	12	12	67.75	48	0.1	82.51	12.9	3865
RELA	12	0	12	12	66.82	3	0.1	82.26	12.89	4035
HMGB3	4	0	4	12	96.11	15	0.111	67.12	12.2	1446
KLF6	5	0	5	12	71.26	5	0.077	71.17	11.85	2843
rno-miR-130b-3p	4	0	4	12	102.1	15	0.1	73.72	12.73	3390
TGFBR3	12	0	12	12	72.17	10	0.091	82.17	12.63	4961
SPAN3N	2	0	2	12	97.5	2	0.077	61.87	11.87	336.6
HEG1	4	0	4	11	95.27	4	0.083	64.75	12.2	1000
rno-miR-206	1	0	1	11	88.84	1	0.083	46.82	10.63	0
TPS3	10	0	10	10	41.29	16	0.1	75.84	12.63	5040
VGLL3	8	0	8	10	97	1	0.091	75.51	12.51	2243
TGFBR2	6	0	6	10	72.33	8	0.091	60.12	12.88	4755
FOSB	4	0	4	10	65.64	14	0.111	65.89	12.24	6322
CYBRD1	4	0	4	10	92.06	2	0.091	60.25	11.88	1638
rno-miR-182-5p	3	0	3	10	95.98	1	0.083	60.18	11.7	188.7
rno-miR-96-5p	3	0	3	10	73.97	1	0.071	49.66	11.17	1167
PTPN9	2	0	2	10	23.91	5	0.077	30.35	10.82	2200
rno-miR-381-3p	2	0	2	10	23.38	8	0.083	42	9.545	3868
rno-miR-21c	1	0	1	10	9.87	2	0.071	33.74	11.69	0
rno-miR-130a-5p	1	0	1	10	100.6	1	0.083	51.93	11.09	0
KLF4	9	0	9	9	60.58	6	0.091	71.69	12.26	3557
EJF1	9	0	9	9	46.74	17	0.1	74.85	12.78	4004
EML1	3	0	3	9	31.86	10	0.091	47.19	10.49	4300
rno-miR-383-3p	3	0	3	9	28.73	2	0.083	39.81	11.63	1175
PRICKLE2	3	0	3	9	64.2	2	0.077	50.36	10.66	579.1
AIF3	3	0	3	9	89.58	1	0.077	54.29	11.06	139.6
JUN	8	0	8	8	73.46	6	0.1	82.17	12.18	3126
PDK4	8	0	8	8	68.43	23	0.091	81.09	12.9	5707
TRAF3IP3	5	0	5	8	16.55	8	0.091	60.96	11.89	2650
MYH10	4	0	4	8	64.42	5	0.111	59.4	12.37	2736
rno-miR-132-3p	4	0	4	8	78.93	5	0.083	70.27	12.33	3638
rno-miR-27a-3p	3	0	3	8	44.47	11	0.1	55.75	11.42	4981
rno-miR-320c	3	0	3	8	19.07	4	0.083	45.68	9.846	1860
SEMA3	3	0	3	8	5.214	3	0.067	40.47	9.201	701.2
rno-miR-424-5p	3	0	3	8	5.407	3	0.067	40.47	9.201	1004
rno-miR-5190-3p	2	0	2	8	84.78	1	0.083	57.3	11.42	114.3
rno-miR-1271-5p	2	0	2	8	69.64	2	0.071	52.36	10.94	213.6
PRNP2	7	0	7	7	45.47	12	0.1	61.93	12.49	1656
rno-miR-129-5p	4	0	4	7	45.43	4	0.083	61.45	11.73	1662
TMOD1	3	0	3	7	77.75	6	0.083	63.86	12.13	1413
rno-miR-301b-3p	3	0	3	7	78.62	3	0.083	63.86	11.93	4814
AURKA	2	0	2	7	27.97	2	0.091	61.68	11.92	421.8
rno-miR-301a-3p	2	0	2	7	93.02	1	0.083	63.86	12.13	1000
rno-miR-139-5p	2	0	2	7	66.45	2	0.083	55.95	11.34	705.3
rno-miR-300	1	0	1	7	17.68	1	0.071	32.63	7.595	0
rno-miR-372-5p	1	0	1	7	17.68	1	0.071	32.63	7.595	0
rno-miR-149-5p	1	0	1	7	17.85	1	0.071	32.63	7.595	0
rno-miR-22-3p	1	0	1	7	89.72	1	0.083	50.04	11.01	0
SELE	4	0	4	6	64.64	14	0.111	62.53	12.33	1302
GOLIA1	4	0	4	6	60.56	3	0.111	52.84	13.07	4079
PPARA	4	0	4	6	41.05	2	0.091	53.58	11.63	1257
ERG	4	0	4	6	22.2	3	0.083	65.06	11.97	1926
ETS1	4	0	4	6	50.49	14	0.1	75.6	12.63	5086
ID1	4	0	4	6	48.6	2	0.083	60.96	12.2	1546
lsa-miR-7c-5p	4	0	4	6	54.78	2	0.083	58.13	12.31	1098
MASP3	3	0	3	6	7.366	3	0.077	48.38	10.61	1110
rno-miR-326	3	0	3	6	68.23	2	0.083	55.95	11.34	2824
FGD5	3	0	3	6	73.17	2	0.091	58.13	11.65	558.9
rno-miR-148a-3p	3	0	3	6	73.33	1	0.083	67.6	12.23	1108
NTN4	3	0	3	6	78.62	1	0.083	67.6	11.62	2018
rno-miR-377-3p	2	0	2	6	29.69	6	0.083	60.89	11.79	2740
rno-miR-199b-5p	2	0	2	6	67.99	1	0.083	60.89	11.61	2000
rno-miR-29a-3p	2	0	2	6	71.48	1	0.083	60.89	11.87	543.2
SUT2	2	0	2	6	5.331	4	0.077	45.43	10.19	842.8
rno-miR-195-5p	1	0	1	6	80.24	1	0.083	57.3	11.42	677.4
rno-miR-4262	2	0	2	6	51.19	4	0.083	57.37	11.62	501.6
rno-miR-9-5p	1	0	1	6	17.7	1	0.083	50.93	11.49	0
rno-miR-181a-5p	1	0	1	6	50.93	1	0.083	50.93	11.49	0
VWF	5	0	5	5	42.75	15	0.1	69.16	12.24	1315
LPL	5	0	5	5	54.01	10	0.091	70.56	12.51	1000
TYMS	5	0	5	5	40.2	15	0.091	65.06	12.84	4959
STAT5A	5	0	5	5	34.29	3	0.1	69.03	12.23	1313
HMOX1	5	0	5	5	45.58	3	0.1	62	12.44	1447
STAT5	5	0	5	5	49.1	6	0.111	74.24	12.71	2575
FRAS1	5	0	5	5	67.63	1	0.077	62.4	11.74	188.3
ACVR1J	5	0	5	5	25.32	1	0.083	52.06	12.56	2120
OLR1	3	0	3	5	73.04	11	0.091	70.04	12.37	3056
PMP22	3	0	3	5	28.61	1	0.083	50.93	11.49	1115
HEY1	3	0	3	5	9.241	3	0.091	55.66	11.23	1753
rno-miR-5195-3p	3	0	3	5	52.77	4	0.083	60.87	11.79	1182
rno-miR-27b-3p	3	0	3	5	25.02	3	0.083	46.1	10.63	1257
rno-miR-342-3p	2	0	2	5	52.25	2	0.071	40.02	9.194	556
rno-miR-454-3p	2	0	2	5	78.55	1	0.083	67.03	12.33	1244
rno-miR-31-5p	2	0	2	5	43.44	2	0.083	60.18	11.79	1168
rno-miR-148b-3p	2	0	2	5	67.98	1	0.083	63.04	11.92	418.4
rno-miR-144-3p	2	0	2	5	76.13	1	0.083	66.44	12.13	1874
rno-miR-29b-3p	2	0	2	5	63.14	1	0.083	60.89	11.79	1674
rno-miR-150-5p	2	0	2	5	4.97	4	0.071	44.55	9.989	862.5
rno-miR-505p-3p	2	0	2	5	57.94	1	0.083	60.89	11.79	1000
rno-miR-181b-5p	2	0	2	5	33.31	2	0.083	61.06	11.89	556.4
rno-miR-199a-5p	1	0	1	5	63.66	1	0.083	46.73	10.47	0
rno-miR-29a-5p	1	0	1	5	57.94	1	0.083	46.73	10.47	0
SLC50A1	1	0	1	5	69.45	1	0.067	48.46	10.68	0
CAV1	4	0	4	4	38.4	21	0.091	77.25	12.73	1673
FOS	4	0	4	4	43.04	5	0.111	62.53	12.72	3819
STAT5	4	0	4	4	36.54	6	0.091	75.27	12.64	1810
CAT	4	0	4	4	57.31	3	0.091	69.16	12.68	1000
YBX1	4	0	4	4	15.08	9	0.083	63.11	11.9	3037
LYVE1	4	0	4	4	52.73	3	0.091	63.09	11.87	765.7
GATA2	4	0	4	4	34.04	3	0.083	52.06	11.1	1311
DUSP1	4	0	4	4	49.33	1	0.1	74.63	12.66	3993
RUNX1	4	0	4	4	35	5	0.1	63.36	11.93	1780
SLC29A1	4	0	4	4	30.22	8	0.091	66.44	12.1	2792
SLC6A4	3	0	3	4	6.21	6	0.077	22.02	10.95	1908
HPGD	3	0	3	4	16.27	3	0.091	60.38	11.7	1223
rno-miR-7c-5p	3	0	3	4	65.15	3	0.083	60.89	11.87	2631
rno-miR-449b	3	0	3	4	50.29	6	0.1	73.14	12.68	2250
rno-miR-3064-5p	3	0	3	4	15.12	6	0.083	60.89	11.92	1000
CSF3	2	0	2	4	22.67	2	0.077	49.73	10.74	556
rno-miR-34a-5p	2	0	2	4	39.86	2	1	52.86	11.25	556
rno-miR-6534-5p	2	0	2	4	12.47	4	0.083	61.33	11.98	1000
HSAT1	2	0	2	4	68.59	1	0.077	56.62	12.28	423.2
rno-miR-103a-3p	2	0	2	4	19.69	2	0.083	61.33	11.91	556
SEMA3A	1	0	1	4	64.4	1	0.067	48.46	10.68	0
rno-miR-330-3p	2	0	2	4	8.824	2	0.083	49.22	10.71	556
rno-miR-3068	2	0	2	4	65.34	1	0.083	60.89	11.4	556
CD4	4	0	4	3	11.2	2	0.067	51.01	10.94	556
lsa-miR-7g-5p	2	0	2	4	38.03	1	0.083	55.11	11.38	62.9
rno-miR-331-3p	1	0	1	4	68.66	1	0.083	50.93	11.29	0
rno-miR-200c-3p	1	0	1	4	51.56	1	0.071	50.09	10.86	0
rno-miR-23b-3p	1	0	1	4	62.43	1	0.071	49.5	10.57	0
rno-miR-478-3p	1	0	1	4	68.66	1	0.071	50.09	10.86	0
rno-miR-497-5p	1	0	1	4	67.87	1	0.071	54.67	11.47	0
rno-miR-29c-3p	1	0	1	4	66.07	1	0.071	54.67	11.47	0
ID3	1	0	1	4	74.81	1	0.077	59.75	11.78	0
EPCAM	3	0	3	3	41.23	2	0.091	65.25	12.08	90.5
EDN1	3	0	3	3	33.15	2	0.083	60.89	11.92	556
NGO1	3	0	3	3	19.72	3	0.091	57.45	11.33	167.8
NFE2L2	3	0	3	3	16.85	2	0.083	61.17	11.8	647.6
SIM1	3	0	3	3	26.29	1	0.083	52.06	12.19	377
TFCP2	3	0	3	3	23.66	1	0.083	64.88	12.08	243.9
rno-miR-7b-3p	3	0	3	3	24.23	2	0.091	71.12	12.48	696.9
ATF3	3	0	3	3	44.47	1	0.1	72.36	12.59	1032
SMAD4	3	0	3	3	26.36	3	0.071	50.84	10.58	1110
PRNP3	3	0	3	3	9.241	3	0.083	60.89	12.32	1674
RNF144B	3	0	3	3	31.84	2	0.091	49.67	10.76	566.8
TBX3	2	0	2	3	21.14	1	0.091	57.53	11.51	149.3
MSX2	2	0	2	3	54.15	1	0.077	53.64	11.03	165.3
rno-miR-431-5p	2	0	2	3	47.93	3	0.1	53.95	11.22	235
rno-miR-876-5p	2	0	2	3	8.773	2	0.083	49.32	10.7	556
CSRNP1	2	0	2	3	8.773	2	0.077	49.32	10.7	1389
rno-miR-106b-5p	2	0	2	3	48.66	1	0.083	56.35	12.23	660.7
ADAMB1	2	0	2	3	35.33	1	0.077	50.09	10.86	0
rno-miR-200a-3p	1	0	1	3	37.96	1	0.1	53.76	11.37	0
FERMT2	1	0	1	3	13.27	1	0.077	49.54	10.91	0
rno-miR-129-5p	1	0	1	3	60.25	1	0.083	50.93	11.29	0
rno-miR-4460	1	0	1	3	32.77	1	0.071	39.35	9.186	0
rno-miR-32-5p	1	0	1	3	51.88	1	0.071	39.35	9.186	0
rno-miR-129-2-3p	1	0	1	3	6.877	1	0.083	50.93	11.29	0
rno-miR-410-3p	1	0	1	3	59	1	0.083	61.38	12.03	0
KIAA1324L	1	0	1	3	26.79	1	0.077	48.68	10.75	0
NEDD9	1	0	1	3	51.07	1	0.077	50.09	11.02	0
rno-miR-204-5p	1	0	1	3	8.973	1	0.083	48.66	10.69	0
SLITI3	1	0	1	3	28.12	1	0.077	49.73	10.73	0
rno-miR-132-3p	1	0	1	3	37.65	1	0.071	41.72	9.86	0
rno-miR-526b-3p	1	0	1	3	56.8	1	0.083	47.91	10.68	0
rno-miR-451-5p	1	0	1	3	8.14	1	0.083	39.81	9.946	0
AGER	1	0	1	2	25.71	2	0.083	65.41	12.14	61.81
MYL9	2	0	2	2	19.2	4	0.091	57.92	11.56	93.65
GKN2	2	0	2	2	16.55	2	0.083	61.38	11.82	149
MMP12	2	0	2	2	23	1	0.083	63.35	11.97	209.2
TOP2A	2	0	2	2	16.68	1	0.083	61.38	11.82	75.75
A2M	2	0	2	2	25.75	2	0.091	63.56	12.05	416.7
FABP4	2	0	2	2	20.7	1	0.091	61.03	11.85	20.49
CD36	2	0	2	2	21.06	1	0.091	61.68	11.85	1976
GATA6	2	0	2	2	19.53	2	0.083	63.86	12.05	100.1
HCAR3	2	0	2	2	20.98	1	0.1	63.21	11.9	23.31
CDH3	2	0	2	2	19.67	1	0.091	57.92	12.48	233.3
ELF3	2	0	2	2	21.69	3	0.1	64.98	12.11	73.11
MMP11	2	0	2	2	27.08	2	0.091	60.12	12.77	838.4
PRC1	2	0	2	2	11.55	2	0.091	58.07	11.64	556
SP2	2	0	2	2	23.49	12	0.1	66	12.2	1321
SASH1	2	0	2	2	5.267	2	0.067	37.93	8.857	556
NR2F2	2	0	2	2	8.022	3	0.083	70.96	10.77	82.29
rno-miR-193a-3p	2	0	2	2	26.99	2	0.083	54.23	11.22	556
SPTBN1	2	0	2	2	5.167	2	0.067	64.2	10.86	556
EPAS1	2	0	2	2	21.69	1	0.091	64.23	12.09	151
HDAC5	2	0	2	2	9.477	5	0.083	53.29	11.14	1368
rno-miR-125a-5p	2	0	2	2	13.53	1	0.071	37.4	8.746	0
rno-miR-330-5p	1	0	1	2	21.17	1	0.083	52.47	11.21	0
FURIN	1	0	1	2	9.167	1	0.067	37.93	8.849	0
ANKRD29	1	0	1	2	46.61	1	0.091	50.97	10.96	0
FBLN5	1	0	1	2	4.312	1	0.077	41.33	9.71	0
rno-miR-296-3p	1	0	1	2	4.67	1	0.071	40.02	9.669	0
rno-miR-136-5p	1	0	1	2	3.675	1	0.071	40.61	9.809	0
rno-miR-133b	1	0	1	2	47.8	1	0.083	54.13	11.29	0
rno-miR-98-5p	1	0	1	2	47.32	1	0.083	54.13	11.29	0
rno-miR-24-3p	1	0	1	2	34.04	1	0.071	50.09	10.86	0
DOLK1	1	0	1	2	13.53	1	0.067	37.93	8.197	0
rno-miR-1197	1	0	1	2	40.78	1	0.071	49.5	10.57	0
rno-miR-582-5p	1	0	1	2	42.78	1	0.071	49.5	10.57	0
rno-miR-16-5p	1	0	1	2	3.33	1	0.063	30.84	8.256	0
rno-miR-489-3p	1	0	1	2	13.89	1	0.071	41.6	9.803	0
rno-miR-505p-3p	1	0	1	2	34.19	1	0.083	47.31	10.66	0
ZFP36	1	0	1	2	5.267	1	0.067	37.93	8.857	0
DACH1	1	0	1	2	7.842	1	0.067	41.9	9.588	0
MS1	1	0	1	2	9.701	1	0.067	41.9	9.588	0
CAV2	1	0	1	2	7.403	1	0.067	39.81	9.118	0
DCN	1	0	1	2	8.621	1	0.067	39.81	9.118	0
HBB	1	0	1	2	4.713	1	0.067	39.81	9.118	0
CDC20	1	0	1	2	5.269	1	0.077	50.29	10.91	0
COL10A1	1	0	1	2	10.92	1	0.067	53.71	11.24	0
ANKRD1	1	0	1	2	11.06	1	0.067	37.4	8.746	0
CPNM	1	0	1	2	11.45	1	0.067	37.4	8.63	0
SFN	1	0	1	2	13.31	1	0.067	37.4	11.63	0
CCND1	1	0	1	2	13.53	1	0.067	37.4	11.63	0
ECT2	1	0	1	2	14.36	1	0.067	38.93	11.78	0
CDCA7	1	0	1	2	14.53	1	0.067	38.93	11.78	0
ETV4	1	0	1	2	12.62	1	0.067	38.93	11.78	0
ADH1A	1	0	1	2	10.36	1	0.077	51.18	11.1	0
PECAM1	1	0	1	2	8.407	1	0.077	51.18	11.1	0
ACADL	1	0	1	2	11.15	1	0.067	35.63	11.59	0
CDH5	1	0	1	2	6.78	1	0.077	51.18	10.97	0
ICAM2	1	0	1	2	6.888	1	0.077	51.18	10.97	0
ADAMTS1	1	0	1	2	7.381	1	0.077	51.18	10.97	0
SLC7A5	1	0	1	2	22.13	1	0.083	54.23	11.29	0
MAOB	1	0	1	2	22.56	1	0.091	69.78	12.46	0
CCL1	1	0	1	2	19.48	1	0.091	69.78	12.46	0
SLC29A6	1	0	1	2	22.46	1	0.091	69.78	12.46	0
SLC19A3	1	0	1	2	22.29	1	0.091	69.78	12.46	0
MIF1	1	0	1	2	21.58	1	0.091	69.78	12.46	0
EDNRB	1	0	1	2	22.58	1	0.091	69.78	12.46	0
MMRN1	1	0	1	2	20.91	1	0.091	69.78	12.46	0
rno-miR-373-3p	1	0	1	2	6.836	1	0.083	55.38	11.48	0
RRAS	1	0	1	2	22.46	1	0.091	60.12	10.25	0
rno-miR-15a-5p	1	0	1	2	2.482	1	0.071	43.17	8.953	0
rno-miR-122a-5p	1	0	1	2	3.501	1	0.083	50.93	10.64	0
RHCU	1	0	1	2	3.96	1	0.077	50.02	10.92	0
rno-miR-374c-5p	1	0	1	2	24.74	1	0.083	59.62	11.75	0
rno-miR-150-5p	1	0	1	2	17.02	1	0.083	59.62	11.75	0
lsa-miR-7f-5p	1	0	1	2	14.24	1	0.083

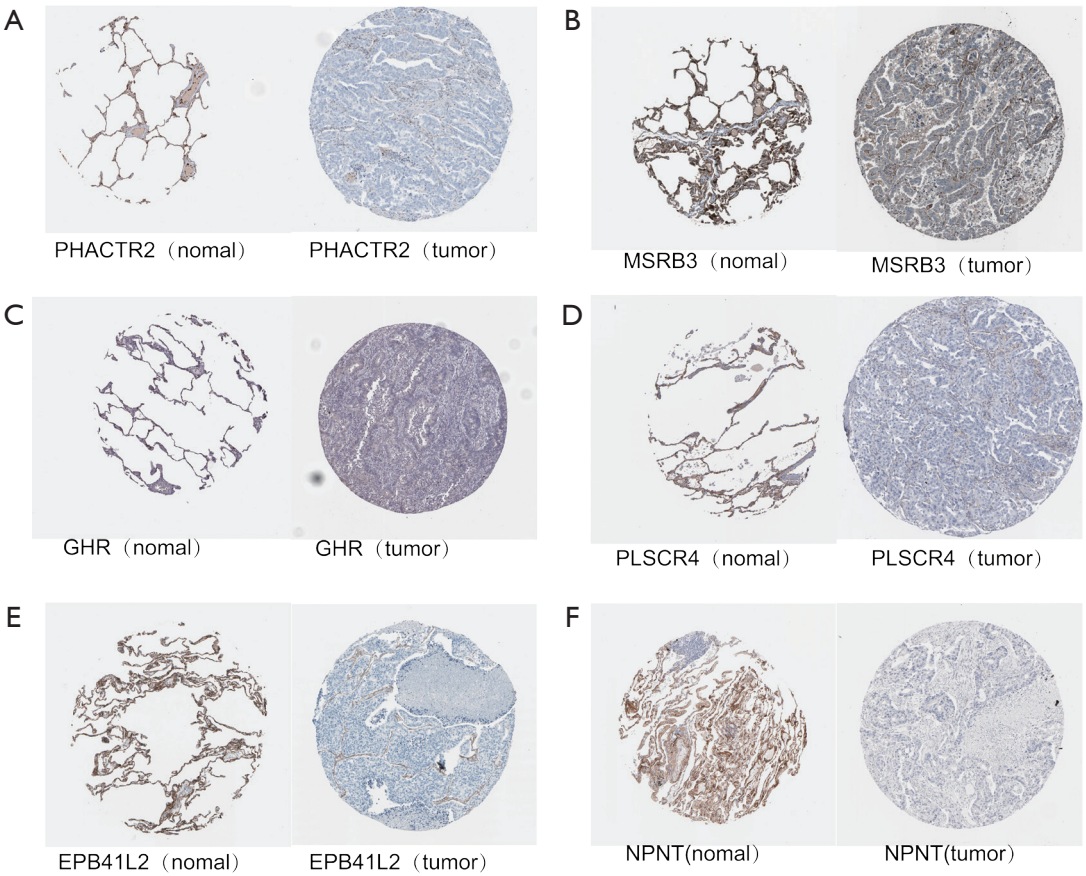

Figure S2 The translational differences of hub gene levels between LUAD tissues and normal lung tissues in the Human Protein Atlas database. The protein expressions were detected by method of SP (streptavidin-horseradish peroxidase) immunohistochemistry. The magnification was ×100. LUAD, lung adenocarcinoma.

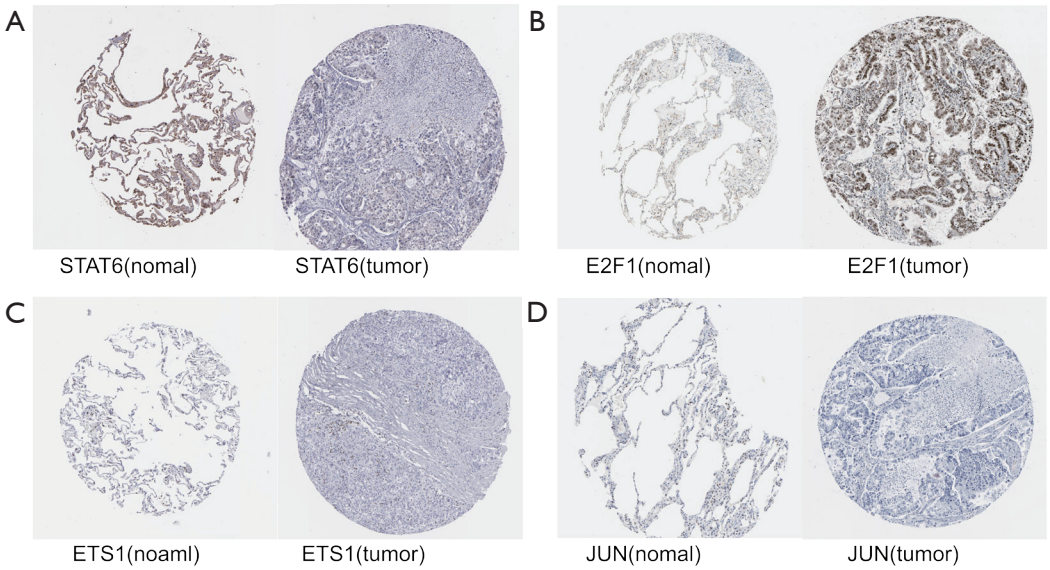

Figure S3 The translational differences of key TF levels between LUAD tissues and normal lung tissues in the Human Protein Atlas database. The protein expressions were detected by method of SP (streptavidin-horseradish peroxidase) immunohistochemistry. The magnification was ×100. TF, transcription factor; LUAD, lung adenocarcinoma.

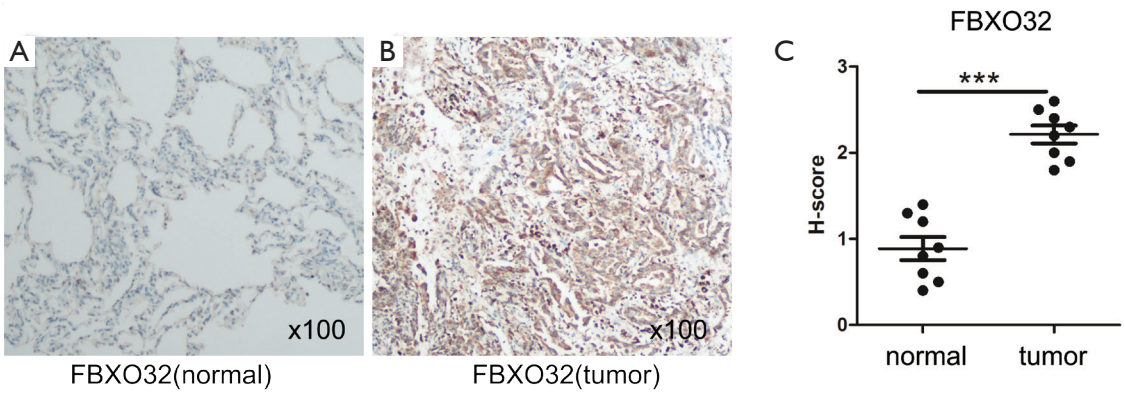

Figure S4 The translational differences of upregulated hub gene (FBXO32). Immunohistochemical results of FBXO32 in normal lung tissues (A) and LUAD tissues (B). The protein expression was detected by method of SP (streptavidin-horseradish peroxidase) immunohistochemistry. The staining score was based on the staining intensity and the percentage of positively stained cells in tissue (C) (***, P<0.001). LUAD, lung adenocarcinoma.

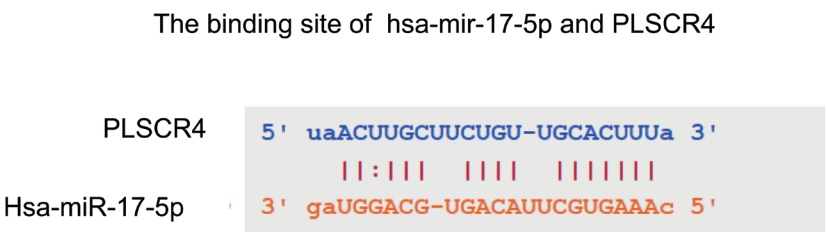

Figure S5 The binding site between hsa-miR-17-5p and PLSCR4.